CERN-SPSC-2005-006
SPSC-P-325
January 10th, 2005

Proposal to the CERN SPSC for AD Physics Starting in 2006 The ALPHA Collaboration (Antihydrogen Laser PHysics Apparatus)

University of Aarhus: *P.D. Bowe, N. Madsen, J.S. Hangst*
University of Calgary: *R.I. Thompson*
University of California, Berkeley: *W. Bertsche, E. Sarid*[†]*, J. Fajans*
University of Liverpool: *A. Boston, P. Nolan, R.D. Page, M. Chartier*
University of Manitoba: *G. Gwinner*
RIKEN: *Y. Yamazaki*
Federal University of Rio de Janeiro: *D. Miranda, C. Cesar*
University of Tokyo: *R. Funakoshi, L.G.C. Posada, R. Hayano*
TRIUMF: *J. Dilling, K. Ochanski, M.C. Fujiwara*
University of Wales, Swansea: *M. Jenkins, L.V. Jørgensen, D.R.J. Mitchard, H.H. Telle, A. Variola*[*]*, D.P. van der Werf, M. Charlton*

1.0 Introduction

The ALPHA collaboration submitted a Letter of Intent (LOI)[1] to the SPSC in September of 2004. The collaboration comprises five groups from ATHENA and five new institutes. It is our intention to continue experimentation with antihydrogen atoms when the AD resumes delivering antiprotons. We thus plan to have a new apparatus ready to produce and study antihydrogen in mid-2006. This apparatus will contain both elements of the decommissioned ATHENA experiment and new components whose purpose is to trap the produced anti-atoms, so that they may be studied spectroscopically. The collaboration has ownership of the ATHENA main magnet, the positron accumulator, and all of the laser hardware developed and installed for ATHENA. We are thus requesting to be permitted to continue to occupy the former ATHENA zone at the AD.

As promised in our LOI, we have completed important plasma physics studies[2] with trapped electrons and a superconducting quadupole magnet. These experiments were designed to determine whether quadrupole fields are suitable for transverse confinement of antihydrogen produced by the interaction of the constituent non-neutral plasmas. We have determined that they are not, and have thus conceived an apparatus to employ a higher-order multipole magnet as the transverse confinement element. We have engaged the Brookhaven National Laboratory (BNL) to construct this magnet, which will be fabricated using a special technique, unique to BNL, for winding superconductor on a small radius bore tube. This magnet will be designed to minimize the material between antiproton annihilation vertices and the detector, so that the imaging capability so important to the success of ATHENA can be retained.

We present below our physics program and the conceptual design of ALPHA.

2.0 Physics Motivations and Goals

Testing of fundamental symmetries is of profound importance in modern physics. Invariance of physical laws under the combined operations, taken in any

[†] Permanent address: Physics Department, NRCN, Beer-Sheva, Israel.
[*] Permanent address: Laboratoire de l'Accelerateur Lineaire, Orsay, France.

order, of Charge-conjugation, Parity, and Time reversal (CPT), is guaranteed in local quantum field theories of point-like particles in flat space time by the CPT theorem[3], under assumptions including Lorentz invariance and unitarity. These assumptions, however, are not implicit in some classes of theories beyond the Standard Model. Recently, there is growing interest in CPT and Lorentz violation, and this is due in part to the development by Kostelecky and co-workers of an extension of the Standard Model[4] that incorporates these violations. Ellis, Mavromatos, and co-workers have also proposed other scenarios of CPT violation involving Quantum Gravity[5]. Any CPT violating effects, if coming from Planck scale physics, would be highly suppressed at low energies, but recent developments in the idea of large extra dimensions[6] might give some hope of observing violations of fundamental symmetries in low energy precision experiments.

Cosmological baryon asymmetry in the universe is normally associated with the famous Sakharov conditions involving CP violation (in baryons or leptons) and thermal non-equilibrium, but alternative models of baryogenesis are possible with CPT violation in thermal equilibrium[7,8]. CPT violation in the neutrino sector[9] is also an active area of current research.

There exist numerous experimental tests of CPT invariance[10], of which the most often quoted is that of the neutral kaon relative mass difference at the level of 10^{-18}. Note however that Kobayashi and Sanda [11], have questioned the significance of dividing the possible mass difference with the mass itself. Given the fundamental importance of CPT symmetry, it should be tested in all particle sectors where precision results can be expected. Comparison of the antihydrogen spectrum with that of its well-studied matter counterpart will provide a unique opportunity for a direct, precision test of CPT symmetry. In particular, the 1s-2s transition in the hydrogen/antihydrogen system offers the potential for an ultimate resolution of 10^{-18} in frequency. Addressing this transition is the main, long-term goal of the AD antihydrogen program.

This goal drew markedly closer in 2002, when ATHENA[12], and later ATRAP[13] synthesized antihydrogen atoms from trapped plasmas of positrons and antiprotons. However, there are many challenges remaining, and we in ALPHA are convinced that the most pressing physics question is whether antihydrogen atoms so produced can be magnetically trapped. The prospect for precision spectroscopy – and thus the very future of these endeavors – depends critically on the answer to this question. Our initial physics program will thus concentrate on answering it. The design of the new apparatus has been developed with this as the main goal, not to be compromised.

An apparatus to trap antihydrogen must contain the elements of ATHENA[14] or ATRAP *plus* superposed magnetic fields for confining the neutral atoms transversely (multipole field) and longitudinally (mirror field) in a minimum **B** configuration[15]. The strategy for attempting to trap antihydrogen was discussed in our LOI and in our presentation at Villars. The steps can be briefly summarized as follows:

1. Production of antihydrogen without neutral trapping fields (commissioning of the apparatus, reproduction of ATHENA and ATRAP results)
2. Production of antihydrogen in the presence of the transverse neutral trapping fields.
3. Study and optimization of various mechanisms for production of antihydrogen in the presence of transverse and longitudinal trapping fields.
4. Demonstration of three-dimensional trapping of antihydrogen.

5. Determination of the absolute efficiency, and the state and phase space distributions of trapped antihydrogen.

The initial emphasis on the transverse fields over the longitudinal ones reflects the fact that the transverse fields break the cylindrical symmetry of the Penning traps used for trapping the charged particles; the longitudinal mirror coils do not[1]. This breaking of symmetry can have very deleterious effects on the stability of trapped plasmas; see Section 3 below.

Once trapping of sufficient numbers of anti-atoms has been demonstrated, we will attempt bound-bound spectroscopy of antihydrogen at the earliest possible time. While it is difficult to design a specific laser experiment until the answers to point 5 above are known, the ALPHA apparatus is designed to allow laser access without another phase of major modifications. We are considering various approaches to antihydrogen spectroscopy and developing lasers in parallel with our trapping efforts. Our laser capabilities will be discussed in Section 8.

3.0 Trapping of Antihydrogen

The main innovations of the ALPHA apparatus concern the systems to trap antihydrogen atoms. We thus consider them in some detail. In the next sections we discuss the experiments at Berkeley that have led us to abandon the idea of using a quadrupole magnet for transverse confinement. We then discuss the best alternative: a higher order multipole magnet. The related technical challenges and their proposed solutions are then covered. We will not repeat in detail the considerations used to design the first generation of antihydrogen experiments, and we assume familiarity with ATHENA and ATRAP. In the following we assume antiproton catching and trapping conditions to be similar to those in ATHENA, and positron performance at least as good as in ATHENA (see section 7.0 below.)

3.1 Quadrupoles and Multipoles – Berkeley Experiments

Antihydrogen atoms are not confined by the electrostatic and uniform solenoidal magnetic fields that confine the positrons and antiprotons from which the antihydrogen is made. Lasers that can trap antihydrogen are not available. Consequently most confinement schemes entail trapping the antihydrogen diamagnetically in a magnetic minimum.[16,17] Such a minimum can be created by superimposing magnetic mirror and multipole coils onto the already present solenoidal field (Figure 3.1). Most commonly, a quadrupole has been suggested for the multipole order.

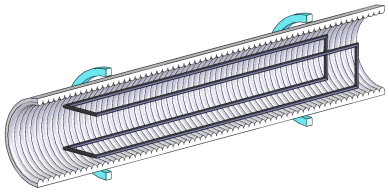

Figure 3.1: Minimum-B configuration created with mirror and quadrupole coils.

With a quadrupole, the total magnet field is given by

$$\mathbf{B} = B_s\hat{z} + \beta_q\left(x\hat{x} - y\hat{y}\right) + \mathbf{B}_{\text{mirror}}\left(r, z\right).$$

The depth of a diamagnetic well for ground state antihydrogen is a mere $0.67\Delta B$ (Kelvin), where ΔB is the increase in the magnetic field magnitude from the formation region to the trap wall (Figure 3.2). The antihydrogen temperature is not well determined, but is probably greater than several hundred Kelvin.[18] At best, only a small fraction of the antihydrogen will be trapped. Maximizing the well depth by creating the largest possible ΔB is thus very important.

Unfortunately, it is not possible to fabricate superconducting magnets with fields any greater than a few Tesla. Confinement of the positrons and antiprotons requires solenoidal fields of a few Tesla. Since the magnetic field at the wall (radius R_w) is the quadrature sum of the solenoidal field and the quadrupolar field, $R_w\beta_q/B_s$ will inevitably be on the order of one to get an appreciable well depth.

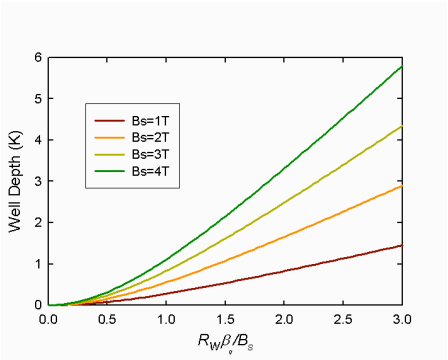

Figure 3.2: Well depth as a function of quadrupole strength.

Unfortunately, multipole fields break the azimuthal symmetry that assures good confinement for the positrons and antiprotons.[19] It is not obvious that these particles can be trapped in the presence of these fields. One set of largely experimental work suggests that it is not feasible,[20,21,22,23] while a theory paper[24] and one experiment suggest[25] that it is. However, all this older experimental work was done at relatively weak solenoidal fields,[20,21,23] or with weak quadrupole to solenoidal field ratios[25]. Only recently[2] have experiments been undertaken at Berkeley at near relevant fields that exhibit clear scaling to the necessary field strengths. These experiments rule out the use of quadrupole fields.

The Berkeley experiments studied the confinement of an electron plasma in the presence of a quadrupole field. Thus, the total magnet field was given by

$$\mathbf{B} = B_s\hat{z} + \beta_q\left(x\hat{x} - y\hat{y}\right).$$

An ensemble of field lines, originating from a circle at the origin, circumscribes an increasingly elliptical figure away from the origin (Figure 3.3).

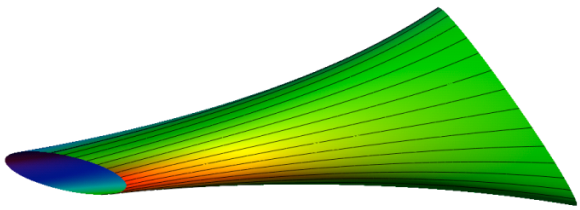

Figure 3.3: The shape circumscribed by magnetic field lines emanating from a circle.

The four extremal field lines, which are located at the quadrant points, follow:

$$r(z) = r_0 \exp\left(\pm \frac{\beta_q z}{B_s}\right)$$

The other field lines rotate towards the extremal expanding field lines as they propagate in $\hat{z}$. Consequently, most field lines expand appreciably.

Field lines starting at radius r_0 can only propagate a distance $z = L$, given by the solution of the equation

$$\frac{R_w}{r_0} = \exp\left(\frac{R_w \beta_q}{B_s}\frac{L}{R_w}\right),$$

before they begin to hit the wall. Since particles tend to follow field lines, a positron or antiproton on one of these field lines will annihilate if it travels the same distance. The average particle radius in the ATHENA and ATRAP experiments was approximately half the wall radius: $r_0/R_w = 0.5$. If a quadrupole of strength $R_w\beta_q/B_s = 1$ had been applied to these experiments, particles traveling more than $\Delta z = 0.69R_w$ would have annihilated on the trap wall.

The electrostatic wells used to axially confine the charged particles are produced by applying potentials to a series of cylinders (see Figure 3.4.) A double electrostatic well (Nested Penning trap) cannot be synthesized with less than five cylinders. But if a cylinder's length is much smaller than its radius, the potentials on the cylinder's wall do not penetrate to the cylinder center. Consequently, the trap length cannot be much less than five wall radii. The traps used in ATHENA and ATRAP were 6.5 (or more) times their wall radii.

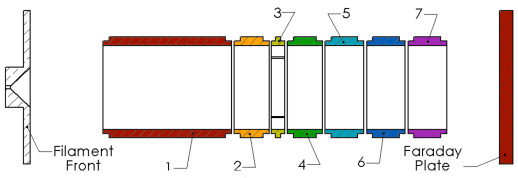

Figure 3.4: The Berkeley electron trap.

Since the traps themselves cannot be short, the particles will travel long distances, particularly during the following phases:

1. *Injection of particles.*
   During the injection phase, particles have to enter the trap from some distance away. The Berkeley experiments demonstrated particle loss during similar injections (see Figure 3.5.) It is very unlikely that particles can be successfully injected into a trap with an energized strong quadrupole. The quadrupole has to be turned on after the particles are injected. Consequently, permanent magnet quadrupoles, which have occasionally been proposed,[22,25] are not feasible.

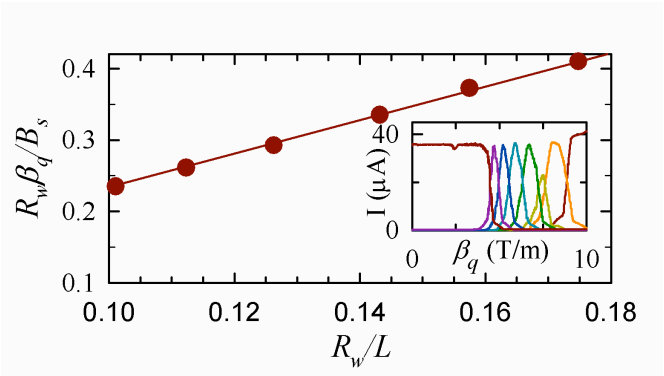

Figure 3.5: (Inset) The beam current collected on successive trap elements, beginning (at $\beta_q = 0$) with the Faraday Plate and ending (at $\beta_q = 9\ \mathrm{T/m}$) with Cylinder 1 (Figure 3.4), as a function of the quadrupole field β_q. Less current is collected on cylinder 3 because it is relatively short. (Main) The normalized quadrupole field that maximizes the current on cylinders 1-6, as a function of the distance of the cylinders from the filament front. All measurements are at B_s=0.2 T and the beam radius is approximately $r_0 = 0.1R_w$.

2. *Positron-antiproton mixing*.
   Both ATHENA and ATRAP formed antihydrogen by pushing antiprotons through the positron plasma. Depending on the details of the process, the antiprotons propagate through three to five cylinders during this process. In the Berkeley experiments a substantial fraction of the particles where lost instantly when $R_w\beta_q/B_s$ approached one. The remaining particles were lost soon thereafter (see Figure 3.6.) Other measurements, shown in Figure 3.7, demonstrate that increasing the solenoidal field while keeping the ratio $R_w\beta_q/B_s$ constant does not reduce the losses.

Charged particles are lost quickly even when they are not being expanded or injected. The plasma column for the "No length expansion" curve in Figure 3.5 was stored in a cylinder whose length was equal to R_w. The column's actual length was closer to $0.3R_w$, short enough that the field lines did not hit the wall. Nevertheless, particles were lost very quickly as $R_w\beta_q/B_s$ approached one. We postulate that diffusion processes, described in Ref. 21, acting in concert with the expanding field lines quickly destroy the plasma. Even antihydrogen production schemes that do not involve mixing[26] will likely fail due to particle loss.

Other measurements demonstrate that these losses are independent of density and temperature. Rotating wall electric fields[27,28] were not sufficient to keep the plasma confined. Harmonic potential wells were not superior.

Taken together, these measurements demonstrate that we cannot make deep neutral wells with quadrupole fields while simultaneously confining positrons and antiprotons.

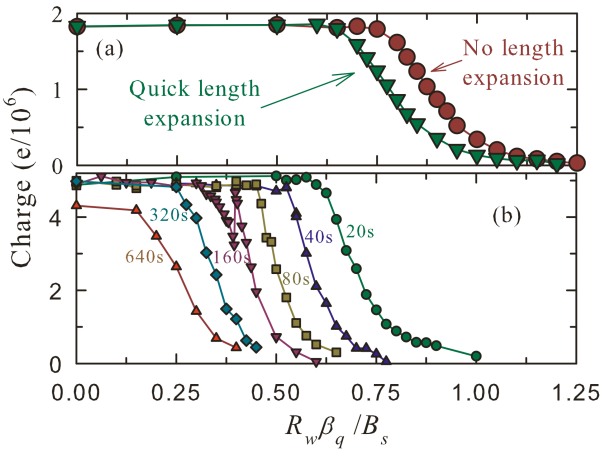

Figure 3.6: Charge remaining in the trap as a function of a quickly-ramped quadrupolar field. The solenoidal field was $0.4\,\mathrm{T}$. The "No length expansion" plasma was stored in a single cylinder of length $1\,\mathrm{cm}$; the "Quick length expansion" plasma was briefly lengthened from $1\,\mathrm{cm}$ to $4.08\,\mathrm{cm}$ while the quadrupole was at full strength. (b) The charge remaining at the indicated times as a function of the quadrupole field. The solenoidal field was $0.4\,\mathrm{T}$, and the grounded trap length was $2\,\mathrm{cm}$.

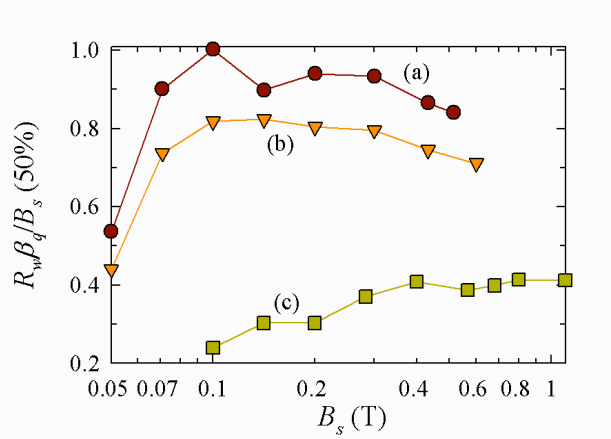

Figure 3.7: The quadrupole field strength at which half the initial ($\beta_q = 0$) charge is lost as a function of the solenoidal field, for a $1\,\mathrm{cm}$ grounded trap length that is (a) not briefly lengthened, (b) is briefly ($2\,\mathrm{ms}$) lengthened to $4.08\,\mathrm{cm}$, and (c) is briefly ($2\,\mathrm{ms}$) lengthened to $7.08\,\mathrm{cm}$. Once the solenoidal field is greater than about $0.1\mathrm{T}$, the loss is approximately independent of the field ratio.

Fortunately, these confinement problems can be alleviated by replacing the quadrupole with a higher order multipole. For a multipole of order s ($s = 2$ for a quadrupole), the field strength increases like r^{s-1}. The field near the axis is greatly reduced as s is increased. For example, the field of a decapole ($s = 5$) is 125 times weaker at $r_0/R_w = 0.2$ than an equal strength (at the wall) quadrupole. By keeping the radius of the charged particles small, the trap can be designed so that the charged particles barely experience the multipole fields, but the neutral antihydrogen is trapped by the multipole field as its strength increases near the wall. This has two

beneficial effects: (1) Diffusion should be substantially lower since the fields in the plasma are lower. (2) The extremal field lines no longer expand exponentially, but instead follow

$$r(z) = \frac{r_0}{\left[1-(s-2)\frac{B_w}{B_s}\frac{r_0^{s-2}L}{R_w^{s-1}}\right]^{\frac{1}{s-2}}},$$

where B_w is the field at R_w. Expansion along field lines (and even injection) should no longer be a problem.

We do not yet have measurements proving that higher order multipoles are definitively superior, but we can make good estimates of their probable effects. Field line expansion sets a firm limit: for $L = 3R_w$ and $B_w = B_s$, fields lines originating at radii of $0.378R_W$, $0.464R_W$ and $0.527R_W$ will hit the wall for an octupole ($s = 4$) a decapole ($s = 5$) and a dodecapole ($s = 6$) respectively. Thus, the charged particle columns need to have relatively small radii. From Figure 3.6, we can estimate that, for quadrupoles, we only achieve satisfactory confinement for $R_w\beta_q/B_s < 0.25$. At a charge radius of $r_0 = 0.2R_w$, the ratio of quadruple field to solenoidal field, $B_w(r_0)/B_s$, is 0.05. If we assume that this figure is primarily set by the strength of the quadrupole rather than by its order, we can extend this figure of merit to higher order multipoles.

Order s	$B_w/B_s = 1$	$B_w/B_s = 2$	$B_w/B_s = 3$
2	0.2	0.4	0.6
3	0.04	0.08	0.12
4	0.008	0.016	0.024
5	0.0016	0.0032	0.0048
6	0.00032	0.00064	0.00096

Table 3.1: The ratio $B_w(r_0)/B_s$ for $r_0 = 0.2R_w$. Green entries satisfy $B_w(r_0)/B_s < 0.05$.

According to table 3.1, octupoles and higher order multipoles are generally satisfactory.

Since the near axis fields get ever smaller with multipole order, one might be tempted to use a very high multipole order. However, the superconducting windings limit the maximum field that the windings can produce to about 2 T for an octupole. This number decreases for higher orders due to practical factors to be discussed in the next section. The magnet inner form and Penning trap electrodes necessarily have a minimum thickness of about 0.1cm each, for a total thickness of $\tau \approx 0.2\,\text{cm}$. Thus, the field at the inside trap wall will be reduced from the maximum field by a factor of $\left[R_w/(R_w+\tau)\right]^{s-1}$ For a typical wall radius of 1.25cm, the field would be reduced by the factors shown in Table 3.2.

s	2	3	4	5	6
$\left[R_w/\left(R_w+\tau\right)\right]^{s-1}$	0.86	0.74	0.64	0.55	0.47

Table 3.2: Field reduction due to wall thickness.

A decapole is perhaps the best compromise.

So far we have only discussed the radial minimum produced by the multipole field. Mirror coils are needed to produce an axial minimum.* The coils must be separated by a distance greater than their radius; otherwise, they will produce an axial field maximum rather than a field minimum. They could either be placed past the ends of the multipole coils, or they could be placed over the multipole coils; because the multipole fields diminish quickly with decreasing radius, the mirror coils cannot be placed under the multipole without sharply diminishing the multipole strength. The detailed interaction between the mirror coils and the multipole coil is complicated because the mirror coils produce radial fields that can cancel the desired radial fields from the multipole, and the multipole coils produce axial fields at their ends. The fields on a bounding surface from a typical decapole are shown below (Figure 3.8):

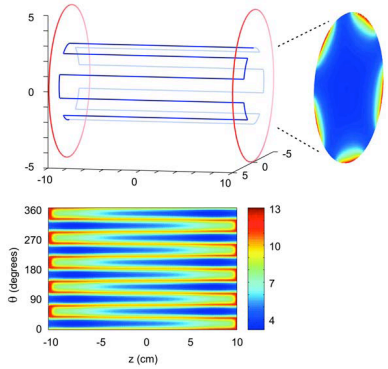

Figure 3.8: Boundary magnetic field values for the configuration shown at top left. All magnetic field values are normalized to the field at the center. The multipole is fifth order with wires at radius 2.5 cm: The mirror coils are of radius 5 cm: The ratio of the current in the multipole to the current in the mirror coils is 1.45. In addition, there is an infinite solenoid, oriented along the configuration axis, which contributes 80% of the field in the center of the trap. The plot at the right shows the field at the end, and the bottom plot shows the ‘‘unwrapped’’ field along on the sides at 90% of the radius of the multipole wires, i.e. a cylinder of radius 2.25 cm: The minimum field occurs about 14% of the way in from the end on the side, and is of magnitude 3.16. The fields were calculated by numerical integration of Biot–Savart’s law in MATLAB.

Further calculations are necessary to finalize the magnetic field design for ALPHA, but the fabrication of the combined multipole/mirror/trap assembly can be discussed quite generally. This is the topic of the next subsection.

* The mirror coil fields affect the field line trajectories discussed above, but numeric calculation show that the effect, though beneficial, is unimportant.

3.2 Fabrication of a Superconducting Multipole

We have concluded that permanent magnets are not a promising solution for our application. The ability to change the multipole field strength and to ramp the multipole on and off are expected to be experimental necessities. The transverse magnetic field geometry of a neutral trap for antihydrogen is identical to that commonly employed for multipole magnets in particle accelerators or storage rings. Since the antihydrogen synthesis trap must operate at liquid He temperatures, it is natural to consider superconducting magnets for ALPHA. Many of the fabrication techniques developed for high field or high gradient superconducting magnets at Fermilab, Brookhaven, DESY and CERN can be exploited here. We have surveyed these and concluded that a specialized process developed at Brookhaven[29] is best suited to the needs of ALPHA.

As noted above, the key to trapping antihydrogen transversely is producing as much field at the wall of the Penning traps as possible. (The probability of trapping antihydrogen atoms for various fields and temperatures will be discussed in section 5 and Appendix A.) For an ideal, infinitely long multipole, the field is produced at the interior of a surface current distribution on a cylinder. The surface current varies as $K_o \cos(s\theta)$, and the field can be described in cylindrical coordinates as:

$$B_r = \frac{\mu_o K_o}{2}\left(\frac{r}{r_c}\right)^{(s-1)} \sin(s\theta) \quad r < r_c$$

$$B_\theta = \frac{\mu_o K_o}{2}\left(\frac{r}{r_c}\right)^{(s-1)} \cos(s\theta) \quad r < r_c$$

where K_o is the surface current density in A/m, and r_c is the radius at which the ideal surface current lies. In this ideal limit, the total field varies as r^{s-1} and the peak field at r_c is independent of multipole order for fixed K_o.

In practice one approximates this current distribution rather imperfectly using azimuthal segments of superconducting cable, resulting in a current distribution having a finite radial thickness. For the purposes of the following discussion, we consider an apparatus with a cross section as shown in Figure 3.9. (A detailed description of the apparatus appears in Section 4.) The configuration below is immersed in a solenoidal field.

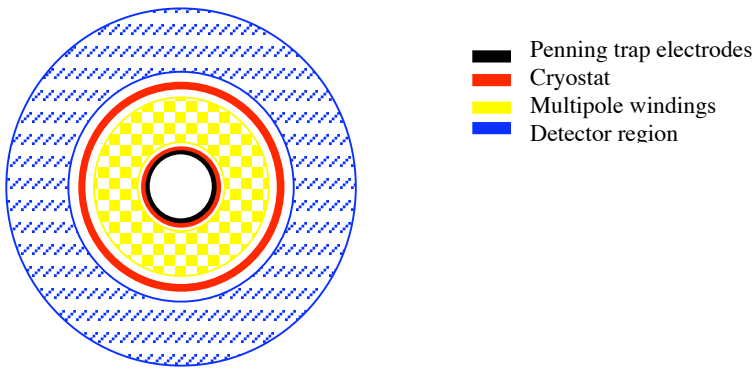

Figure 3.9: Schematic cross section of experimental elements

The maximum *effective* K_o will be limited by the critical current in the superconductor at the field of interest and by the radial extent of the superconductor used. The technical challenge for our application is thus to pack as much superconductor as close to the Penning trap radius as possible. This is somewhat problematic for antihydrogen synthesis experiments, as the typical Penning trap radius used to date is about 1 cm. This size is very compact compared to the transverse dimensions of most superconducting accelerator magnets (e.g., LHC has typically a 27 mm bore radius.) Other practical considerations such as the minimum bend radius of the superconducting cable will also figure strongly in the ultimate design, particularly for higher order multipoles. The geometry for production of multipole fields *precludes having a vertex detector between the multipole and the Penning traps*. The detector must be outside of the multipole windings as in Figure 3.9. One would thus like to minimize the material in the magnet between the Penning electrodes, where unconfined antihydrogen will annihilate, and the annihilation vertex detector.

The Brookhaven Superconducting Magnet Division has developed a technique for winding superconducting cable or wire onto small diameter cylindrical forms. The technique is similar to wire bonding onto silicon; it uses ultrasonic energy to place the cable onto a plastic substrate. Figure 3.10 shows the apparatus in the process of winding a coil. Coils are wound one layer at a time and reinforced with fiberglass

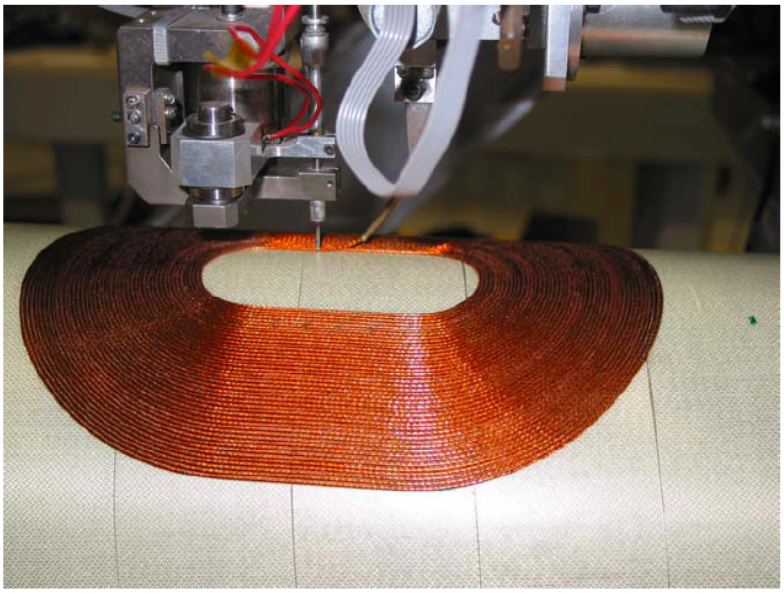

Figure 3.10: The BNL magnet winding apparatus

and epoxy substrate. There are no metal collars or dense support structures. The technique allows for co-axial placement of different magnet types (dipoles, multipoles, or even solenoids) in different radial layers. Brookhaven will supply ALPHA with an assembly consisting of the multipole and the mirror coils wound on a cylindrical tube that will also serve as the inner cryostat wall.

3.3 Multipole Field Considerations

We have studied possible transverse field configurations for Brookhaven magnets using the ROXIE[30] program developed at CERN. The ultimate design will be finalized at Brookhaven, in order to be compatible with their computer-controlled

winding machine, but the general design features and trade-offs discussed below take into account all of the known constraints of their process. Note that, unlike the accelerator community, we are not overly concerned with field quality for our magnet. The goal is to make a multipole with the largest possible field at the trap wall.

Figure 3.11 shows a calculational model (ROXIE) of a superconducting decapole. Each square current element represents a superconducting cable characterized by the critical curves in Figure 3.12. Note that, as mentioned above, the total field at the conductor will be the quadrature sum of the transverse field due the multipole itself and the field from the solenoid. Depending on their strength and

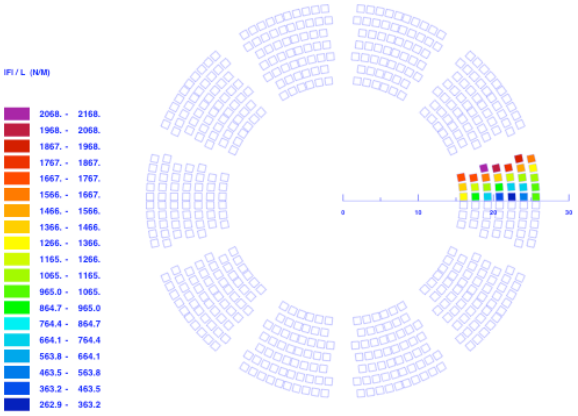

Figure 3.11 ROXIE output for a decapole magnet. The colors show magnetic force per unit length. The field for this seven layer magnet is about 2 T at the inner conductor radius.

placement, the mirror coils may also contribute significant fields at the multipole superconductors. The modeling problem for maximizing the multipole field while avoiding quenches is thus an intricate 3-D one. The issue of magnetic forces on the multipole, due to its own field, the field of the external solenoid, and the field of the mirror coils is also being studied but is not expected to be prohibitive. Brookhaven engineers will design the coil package with all forces taken into account and supported as necessary.

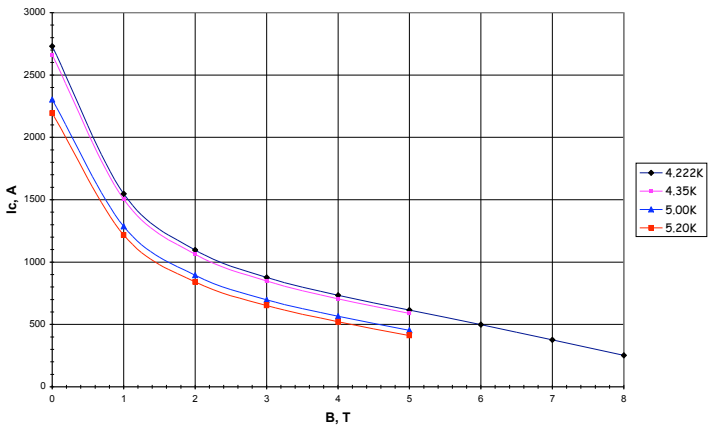

Figure 3.12: Critical current *vs*. magnetic field at various temperatures for typical conductor used in BNL magnets.

As we are also interested in minimizing the multiple scattering of charged pions from the antiproton annihilation, the total thickness of the multipole coils should be minimized. Figure 3.13 shows how the field in a typical decapole varies with the number of layers of superconductor wound. Each layer of winding has a radial extent of about 1.5 mm, including superconductor, insulator, and structural substrate and reinforcement. The inner radius of the magnet in this example is 15.5 mm, which corresponds to a Penning trap inner radius of about 13 mm. The magnet radius is also a variable to be optimized. Larger radius magnets can be fabricated with a larger effective K_o, since the ratio of the radial extent of the windings to the radius of the magnet decreases with radius. Larger radius magnets may also have more turns per pole without violating the minimum bend radius criterion for the cable.

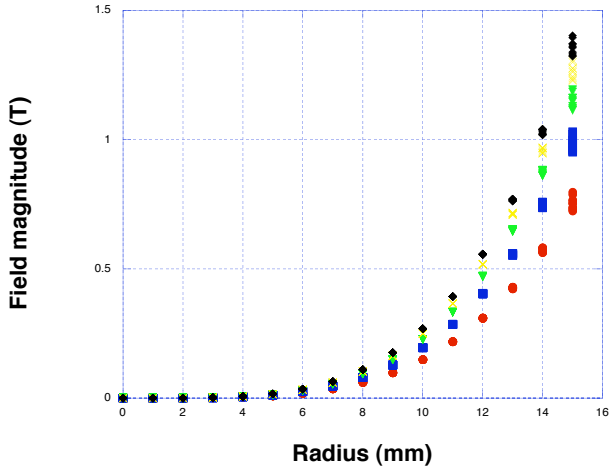

Figure 3.13: Magnetic field vs. radius for decapole magnets wound with two (red) to six (black) layers of superconductor. The spread within a color represents the field variation at different azimuths. The magnet is based on a 15.5 mm radius form.

Since the critical current in the multipole depends on the *total* field magnitude, the peak multipole field will be a function of the magnitude of the solenoidal field employed. We expect to achieve a multipole field strength of about 2 T at the Penning trap electrode inner radius for a solenoidal field of 2 T. Mirror coils that add 2 T to the solenoid are not difficult to wind in extension of the multipole. In fact, the ends of the multipole can be wound in such a way as to contribute a reasonable fraction of the mirror field.

As shown in Figure 3.2 above, the potential well depth (in K) depends on the solenoid and multipole fields as follows:

$$U = \frac{\mu(\sqrt{B_W^2 + B_s^2} - B_s)}{k_B}$$

where B_W is the multipole field at the wall, μ is the antihydrogen magnetic moment, and k_B is Boltzmann's constant. It is thus intriguing to consider lowering the solenoidal field in the neutral trapping region to maximize the well depth. ATHENA used a solenoidal field of 3 T for catching and trapping the antiprotons from the AD. Lowering this field could have profound consequences for the number of antiprotons

caught, the synchrotron cooling time of electrons and positrons in their traps, and many other plasma parameters. An alternative might be to capture and accumulate antiprotons and positrons at high field and then transfer them to a lower field for mixing and trapping of neutrals.

Using the Brookhaven winding technique, this could be achieved by extending one of the mirror coils to form a solenoid to one side of the mixing region. See Figure 3.14. The fringe field of this solenoid would serve as the axial mirror to this side of the multipole. The external solenoid could then be operated at say 1 T, with the inner one providing an additional 2 T for catching and cooling of pbars. The pbars could then be transferred to the 1 T region for mixing with positrons. Particles would be transferred without ever leaving a high magnetic field. Obviously the particle densities will go down when they are transferred, but this effect could potentially be lessened by the application of a rotating wall electric field[27,28]. We are currently investigating all of the plasma physics and antihydrogen formation implications for this scenario. The field configuration will be frozen by the end of January 2005, and fabrication at Brookhaven can begin immediately after that. We expect that the fabrication will take about eight weeks.

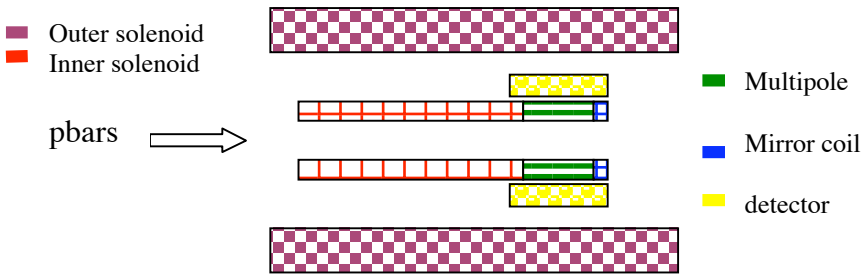

Figure 3.14: Magnet configuration with two solenoids, a multipole and a mirror coil.

4.0 Trap Cryogenic and Vacuum Considerations: Conceptual Design

The experimental power provided by spatial and temporal antihydrogen detection cannot be overstated. One of the core features of the ALPHA design has been the decision to retain this detection capability (see Section 6) when adding a new multipole magnet to trap antihydrogen. Furthermore "open" vacuum system access for high positron numbers and lasers should not be compromised. This involves several design challenges, but also presents some opportunities.

The magnet and detector must be mounted coaxially around the formation and trapping region. From trap depth versus field strength considerations and the corresponding multipole design arguments presented above, it is clear that the multipole magnet should be at a smaller radius than the detector. This introduces more scattering material between the annihilation surface (the trap wall) and the detector, compared to the situation in ATHENA.

The multipole magnet is superconducting and must be kept at liquid helium temperature. This presents difficulties for the successful operation of an adjacent silicon detector over a long period. The ATHENA detector, which operated at 140 K, showed significant deterioration in several of the silicon modules over the period of a single beam time (5 months). The cause of this loss is thought to be cryogenic operation.

The detector is a source of heat, which can act as a thermal load on the trapping region. Achieving cryogenic temperatures in the trapping region is critical to ensure good vacuum. One of ALPHA's experimental advantages is a vacuum system which is "open" at one end. By this we mean that there is no permanent barrier between the antihydrogen formation region, the positron accumulator and the area in between. This gives access to very high numbers of positrons at a high repetition rate and greatly facilitates laser access to the formation region. However, in order to achieve high vacuum in the antihydrogen formation region, the trap electrodes and the inside surface of the trap vacuum chamber must be kept at or very close to the temperature of liquid helium, 4.2 K. Furthermore cooling the antiprotons and positrons as much as possible should minimize the kinetic energy of the antihydrogen formed.

We have developed a novel design concept (Figures 4.1,4.2), which avoids deleterious effects due to the introduction of the multipole magnet, while seizing the opportunities provided by the unique BNL magnet fabrication technique. The key features of this design are the combination of the cooling systems for the trap vacuum and the multipole magnet as well as the operation of the detector at room temperature. In this design the mounting support of the magnet combines several other functions. It is also the inner wall of the helium vessel cooling the magnet Dewar, the vacuum barrier for the trap electrodes, and the cooling surface for those electrodes. An obvious advantage is that only one helium system is needed. Furthermore the total thickness of scattering material in this region will be reduced by ca. 3 mm of copper equivalent. The magnet helium vessel will be surrounded externally by an 80 K thermal shield and inserted in a Dewar with the external wall temperature at 300 K. This thermally decouples the magnet from the detector, which can now operate at 300 K

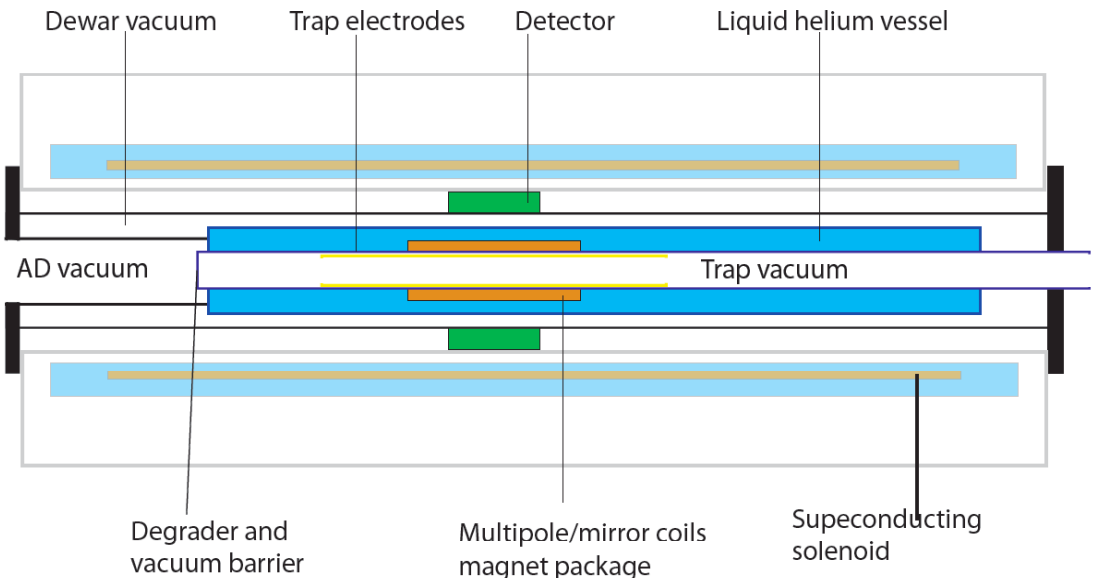

Figure 4.1: Axial view of trap, magnet and detector assembly in the superconducting solenoid. The drawing is to scale although the vertical dimension has been blown up by a factor of two for clarity. Only core components are shown. End coils, 80 K shield, cryogen tubing, pumping ports, trap and detector cabling are not shown.

The feasibility of this system is based on experience at BNL. A Dewar, constructed for DESY in Hamburg, has internal and external radii at room temperature. The total wall-to-wall thickness of the Dewar is 25 mm. In our case we choose to keep the internal radius at helium temperature and thus dispense with the inner 80 K shield and Dewar vacuum container. Note that care will have to be taken to minimize the heat load along the axis of the system.

A magnet of similar dimensions to the one proposed here was built for BEPCII[29] in China by BNL. The total heat load on the helium vessel is 14 W. A particular difficulty with the DESY and BEPCII magnets is that they are cantilever mounted on one external flange and thus require internal fiber reinforced polymer supports between the magnet tube and the external wall of the Dewar. The supports have to be substantial to withstand the forces between the magnets, and 12 W of the heat leak load was due those supports. In ALPHA's case (see figure 4.1) access is possible to both ends of the assembly and these can be fixed to the flange of the superconducting solenoid magnet. The magnet can thus be supported axially where the heat paths are very long as opposed to radially, where they are short. The heat load on the helium vessel of ALPHA's multipole will be substantially lower than that on the BEPCII vessel.

Figure 4.2 is a cross-section through the antihydrogen formation region. The new assembly fits in the 140 mm bore of a superconducting magnet. The sketch shows 6 layers of superconductor, which is the maximum number anticipated.

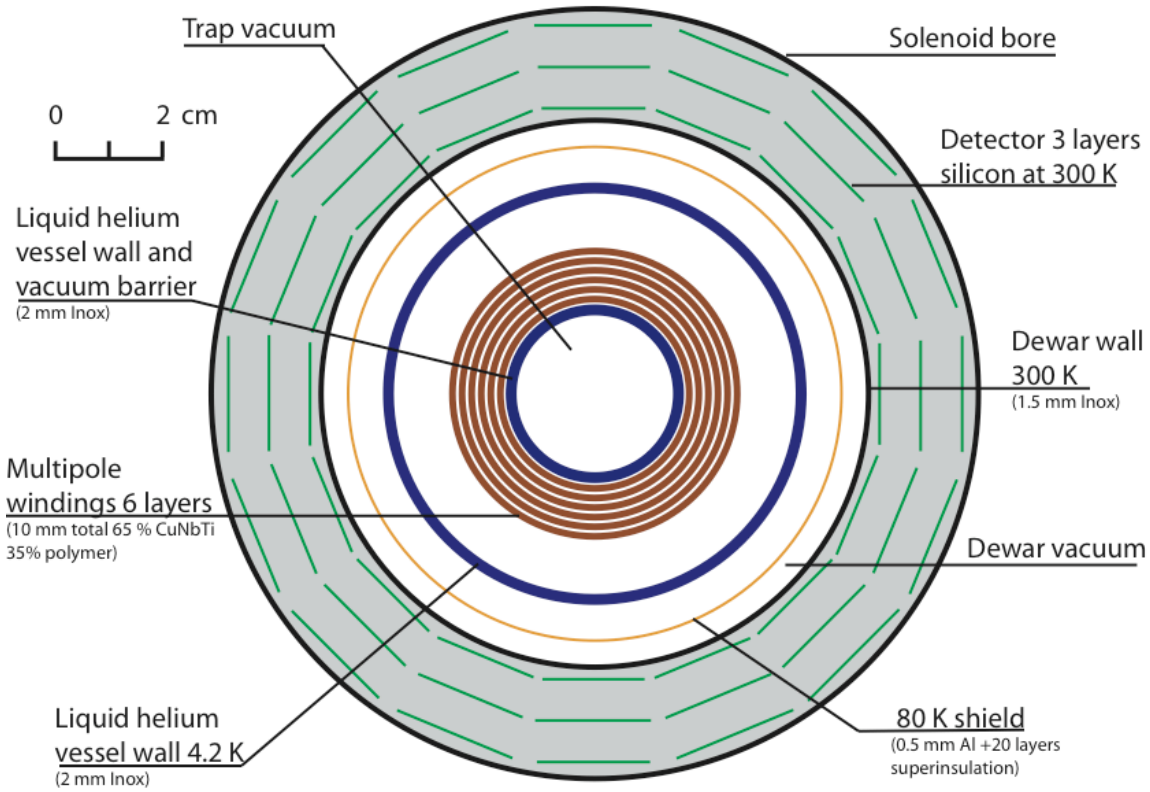

Figure 4.2: Cross section of experimental geometry through the antihydrogen formation and trapping region. All dimensions except for silicon strip thicknesses are to scale.

The material thicknesses for the helium vessel and Dewar are realistic and conservative. They are based on the same strength and thermal radiation analysis in

the BNL BEPCII design report. In order to safely accommodate magnet quenches the helium vessel for the multipole magnet is a pressure vessel. The BEPCII rating is 20 bar. In the case of ALPHA the inner and outer radii are smaller by a factor 5 and 3 respectively while the length of the inner tubes are similar. The thicknesses of the inner and outer vessel walls are shown as 2 mm in each case in Figure 4.2. This gives a margin of safety of a factor of three at 20 bar for the inner vessel and a similar factor for the outer vessel. However the windings are held on the inner vessel wall in compression with glass fiber tape and the trap electrodes are located in this tube. There are more constraints, other than avoiding pressure failure, on the inner tube. In order for the trap electrodes and magnet to be in good alignment the inner tube must maintain its shape. Therefore the thicknesses have been conservatively left somewhat over dimensioned. Nevertheless the total thickness of scattering material between the annihilation surface and the detector is not greater than 12 mm copper equivalent.

Note that in the design concept presented here we have not exhausted the advantages of this new technique and the newly available geometries that open up through it. BNL have constructed systems with several different magnets in the same helium vessel. For instance BEPCII consists of a quadrupole, two dipoles a skew quadrupole and a three-part antisolenoid. Two new possibilities in particular are attractive.

Incorporating the main solenoid in the same volume would only require 3 or 4 extra layers for a 3 T field, which is what is used at present. This would greatly improve the access to the apparatus. In particular the detector could then sit on the outside of the apparatus, opening the possibility of having an external quadrupole at the same radial position but axially offset. One could then alternate between quadrupole and detector operation. Alternatively a quadrupole could be incorporated into the multipole volume, at the expense of detector resolution.

Although it has been shown that multipoles are greatly favored for the initial trapping, the resulting radial trapping area is increased, substantially reducing laser overlap with the trapped antihydrogen atoms. Turning on a quadrupole once the atoms are trapped would be a considerable experimental advantage.

5.0 Antihydrogen Temperature and State: Trapping Considerations

There is strong evidence from ATHENA[31], ATRAP[18] and theoretical simulations[32] that the antihydrogen produced is not as cold as one might like. That is, its kinetic energy, or temperature, on formation is not that characteristic of the temperature of the positron plasma. ATRAP, which uses a technique in which the antiprotons are repeatedly driven through a positron cloud[33], finds antihydrogen kinetic energies as high as 210 meV[18], as measured using their field ionization technique[18,33]. ATHENA, who allow the antiprotons to cool and mix with a positron plasma in a nested Penning trap in a single 3-minute cycle, and detect all antihydrogen which survives the various electric fields within their traps using a purpose-built annihilation detector[14,34], have deduced that the spatial distribution of antihydrogen atoms is independent of the positron temperature and is enhanced in the axial direction. They were able to assign *lower* limits to the antihydrogen temperature of 150 K along the axis of the trap and 15 K perpendicular to it[31]. The unavoidable conclusion of the ATHENA study is that the antihydrogen is not formed under conditions of thermal equilibrium between the positrons and antiprotons. Furthermore, this observation is probably the cause of the unexpected dependence of the antihydrogen formation rate on positron temperature as previously reported by ATHENA[35].

The long-term goals of ALPHA, as outlined in Section 2, involve precision spectroscopic comparisons of hydrogen and antihydrogen. This can only be achieved by trapping cold antihydrogen, and this is one of our central aims (see section 2). Clearly this effort will be severely compromised if the antihydrogen temperature is significantly higher than the magnetic well depth. In this case few anti-atoms will be trapped. Thus, alternatives (to the antiprotons through positrons) recombination scenarios need to be considered.

There are a number of options open to ALPHA, some of which use antiproton-positronium collisions[36]. In particular, collisions involving excited states of positronium are advantageous, since interaction cross sections are high and the antihydrogen recoil energy is negligible. This is an area pioneered by members of ALPHA[37,38], and recently exploited by ATRAP[26,39].

The ATRAP experiment, which utilizes a double-charge exchange scheme involving highly excited cesium atoms[26,39] is probably over-complex. It is likely that similar results can be obtained by producing magnetized Rydberg positronium (Ps*) by dumping the ALPHA positron plasma onto a degrader foil and allowing the Ps* to interact with the trapped antiprotons. Around $2\text{x}10^{-3}$ of the positrons incident on the foil should emerge as Ps*[40], which will be transported, magnetized, with unit efficiency along the axis of the traps. The number of antihydrogen atoms, N_{hbar} produced can be estimated from

$$N_{hbar} = N_{Ps^*} N_{pbar} \sigma$$

where N_{Ps^*} is the Ps* flux, N_{pbar} is the antiproton area density (about 10^4 cm^{-2}) and σ is the antiproton-Ps* cross section for antihydrogen formation. We assume the latter to be geometric in size and based upon the estimates of Estrada *et al.*[40] to be $> 10^{-8}$ cm^2. Inserting values into the above equation one finds that at least 40 cold Rydberg antihydrogen atoms will be produced for every 3-minute positron accumulation cycle. This timed flux should be readily detectable. Work on magnetized Ps* production will take place throughout 2005 in a separate project at Swansea, and also perhaps at CERN.

A similar outcome may be achieved by merging electron and positron plasmas in the strong magnetic field of the ALPHA Penning traps, as in Figure 5.1. The mixing technique would mimic that already demonstrated for antihydrogen formation, however now the electrons would also self cool, and to efficiently combine with the positrons to form Ps* would have to be at a similar velocity to the positrons. Thus, conditions closer to thermal equilibrium between the mixing species would ensue, leading to thermal, or near-thermal Ps*. Again, it is expected that very high-lying states will be magnetized and confined by the strong magnetic field, though special attention will need to be paid to the electric fields they encounter. Lower lying states may not be confined by the field, such that it would be wise to hold the antiprotons in close proximity to the electron/positron cloud, perhaps immersed in the electrons.

If similar numbers of positrons and electrons are merged and the recombination rates can be obtained by scaling those for antihydrogen formation[41], then instantaneous rates close to 10^7 Ps* s^{-1} can be envisaged. Thus, all the positrons will be consumed within a 10-20 s period. Calculating the expected antihydrogen formation rates here is more difficult, since the Ps* state distribution, and hence the

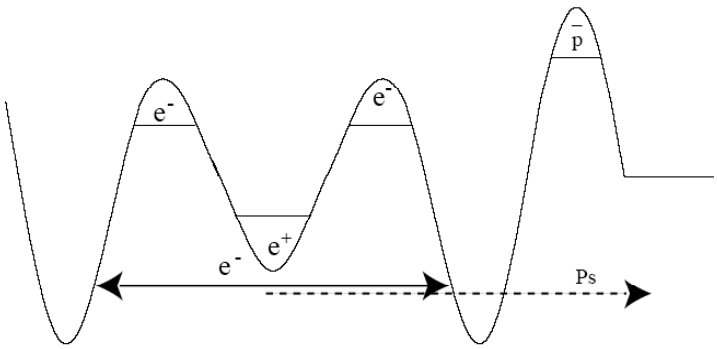

Figure 5.1: Nested trap scheme to produce positronium, which can then drift into the antiproton plasma to produce antihydrogen.

interaction cross section with the antiprotons, is unknown. Experiments with merged electron and positron plasmas will be undertaken by ALPHA during the shutdown period.

A third, and perhaps the simplest method to ensure the production of cold antihydrogen would be to reverse the "polarity" of mixing. Instead of injecting the antiprotons with several eV of kinetic energy into the positron plasma[12], it might be feasible to keep the antiprotons stationary in their trap (perhaps with a few electrons to guarantee that they were cooled to the ambient) and inject the positrons into this region. The positrons will self-cool in the strong magnetic field and presumably antihydrogen formation will ensue. We are considering the effects of decreased positron density to try to evaluate the feasibility of this process, but it is perhaps easier to just investigate it experimentally.

Initially it would make sense for ALPHA to start with the standard nested scheme already tried and tested by ATHENA and ATRAP. Apart from producing antihydrogen that may be too hot to be captured, a large fraction of the antiprotons also separate axially into the side wells[35]. The process responsible in ATHENA seems likely to be field-ionization of Rydberg antihydrogen by the fields comprising the side wells of the nested trap, as the phenomenon is absent without positrons. This has recently been observed to be the case in simulations by Robicheaux[42]. Most likely the antihydrogen formed during the initial burst in formation, as observed by ATHENA, cannot be trapped. However, at a later time the side wells may be raised adiabatically to slowly introduce the antiprotons to the positrons. This simple method is a straightforward extension of the tried-and-tested procedures of ATHENA and ATRAP and if applicable would greatly simplify the overall procedure.

At this point it should be re-emphasized, that the spatial distribution of annihilations, analyzed as done in reference 31, is an important tool for diagnosing the relative success of different schemes. The magnetic field designed to trap the antihydrogen will, in the initial attempts at least, work as an antihydrogen deflector, and by adjusting field strengths may be used as a combined quantum state and kinetic energy filter for antihydrogen. The influence of the magnetic field on the path of an antihydrogen atom will depend on its quantum state and kinetic energy. This path change will in turn manifest itself as a change in the spatial distribution. Being able to detect the spatial distribution is therefore a powerful diagnostic for detecting the

influence of the applied magnetic field on the antihydrogen formed, as well as being a strong tool in determining conditions in the formation region and separating out antiproton-only losses as previously done in ATHENA[43]. Vertex detection will be discussed in greater detail in Section 6.

In Appendix A we calculate the fraction of antihydrogen that one may capture depending on temperature and **ExB** drift velocities of the plasmas. As was pointed out by ATHENA in reference 31 the antiprotons will rotate with the positron plasma due to the strong radial electric field from it. This gives each antihydrogen created additional kinetic energy. Thus, using a dense positron plasma reduces the fraction of antihydrogen that may be caught. We find that, assuming a trap depth of 0.5 K we would capture 5% of antihydrogen formed at 4 K. If they were formed in a plasma identical to the ATHENA plasma, with a density of 1.7×10^8 cm^{-3}, this fraction would be less than 0.1%. It may thus be desirable to reduce the positron density in the final scheme, or use positronium as the intermediary, as in some of the schemes discussed above.

Reducing the positron density may have the side-benefit of changing the relative strength of the two processes believed to be responsible for antihydrogen formation in favor of the radiative process. The two formation processes usually expected to play a role are the radiative process, where excess momentum is carried away by a photon, and the three-body process, where it is carried by an extra positron. Enhancing the contribution of the radiative process is of interest as this process favors formation of antihydrogen in low quantum states. The three-body process favors weakly bound high quantum states, and simulations indicate that the states formed in a nested scheme are even more weakly bound than assumed in standard theory[32]. The radiative process may be additionally enhanced by laser light, as discussed in section 8, which if successful would be the first direct interaction of atomic antimatter with laser light.

This leads us to a final issue; the quantum state of the formed antihydrogen. The trap depth is proportional to the electron magnetic moment, which is given by

$$\mu = \beta(l + 2s),$$

where l is the orbital quantum number, s the electron spin and β the Bohr magneton. Antihydrogen formed in weakly bound states may have large angular momentum and see a deeper magnetic well, and they may therefore be trapped even when created at higher temperatures. This may be a significant advantage in the first attempts to trap antihydrogen. Ultimately we will only be interested in the ground state. These states can only be trapped if very cold, and it will therefore be necessary to either make cold antihydrogen in this state or to cool and de-excite warm antihydrogen created in more weekly bound states. We have above described how ALPHA will achieve this goal by trying a range of different methods.

6.0 Antiproton Vertex Detector

6.1 Introduction

The capability to detect the vertex position of antihydrogen annihilations was an important feature of ATHENA, not only for the identification of cold antihydrogen production[12], but also in the developments leading to the first production[43]. Having

real time images of antiproton losses was absolutely essential as a diagnostic when optimizing the trapped particle manipulation in a nested Penning trap.

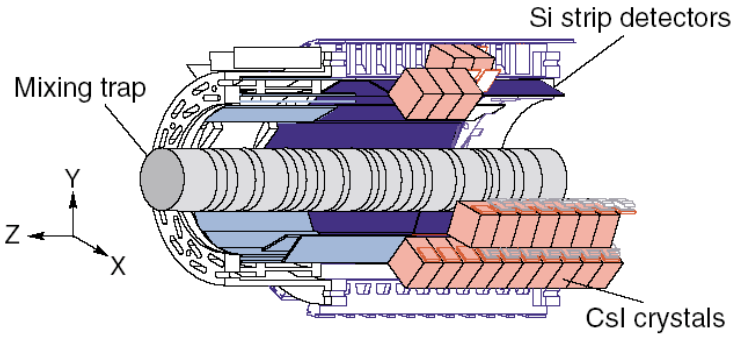

Figure 6.1: Schematic view of the ATHENA antihydrogen detector[34]. Two layers of double-sided Si strip detector and 192 CsI crystals surround the trap region. A 1.65 mm thick copper vacuum wall, between the trap and the detector, is not shown in the figure.

As we enter the unexplored regime of neutral anti-atom trapping, we believe it is crucial to retain the vertex imaging as a diagnosis tool. There exists very little experimental information on the behaviour of trapped, charged particles in multipolar magnetic fields. We will likely encounter unexpected new effects. Given the situation, the importance of real time imaging, together with other plasma diagnosis techniques developed for ATHENA[44,45], cannot be overstated.

We note further that vertex detection capability will play an important role in the future phases of ALPHA. Even after stable trapping of neutral antihydrogen atoms is achieved, performing spectroscopy measurements with few atoms will be extremely challenging, given the expected low signal rates. A clean vertex determination will help demonstrate laser transitions of anti-atoms such as photo-ionization, and can discriminate against possible sources of background.

6.2 The case for vertex detection

In order to further illustrate the power of the vertex detection, we give in this section some examples from the experience in ATHENA. Figure 6.2, taken from the first report in *Nature*[12], shows the difference in the vertex distributions between production data (cold mixing) and the control data (hot mixing). This provided an important piece of evidence for establishing the first production of cold antihydrogen atoms. Subsequent analyses using simulated vertex distributions showed that about 65% of annihilation events in Figure 6.2 (a) are due to antihydrogen and the rest due to background[41].

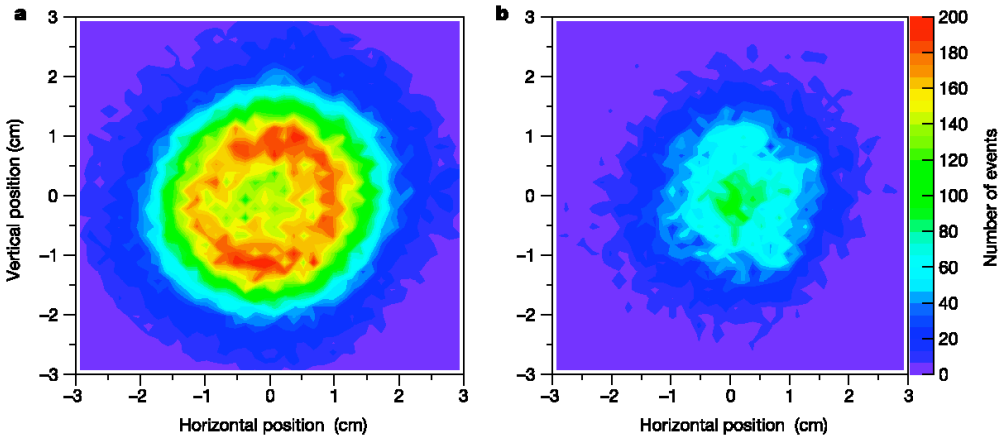

Figure 6.2: X-Y distribution of antiproton annihilation vertices for (a) cold mixing and (b) hot mixing, obtained with the ATHENA detector. Both plots are normalized to the same number of mixing cycles. Enhanced annihilations on the trap electrodes (inner radius 1.25 cm) in (a) indicate antihydrogen production, whereas annihilations of the central part in Fig (b) represent antiproton annihilations on residual gas or ions.

It should be stressed that detecting only antiproton annihilations, for example by external scintillators, is not sufficient evidence on its own for antihydrogen production, because of the existence of particle loss processes in the trap. Figure 6.3 further illustrates the importance of spatially sensitive detection. The axial vertex distributions are compared for the standard cold mixing and the "mixing" without positrons. A clear difference is observed. Suppression or inhibition of antihydrogen production due to causes such as plasma instabilities, vacuum deterioration, or electrode malfunctions are sometimes otherwise difficult to identify, but they would show up immediately in the vertex distributions, allowing rapid diagnosis of the system. An incomplete removal of the electrons (which are used to cool antiprotons in the first step of the mixing cycle) from the trap results in the vertex pattern similar to Figure 6.3 (b) indicating suppressed antihydrogen production.

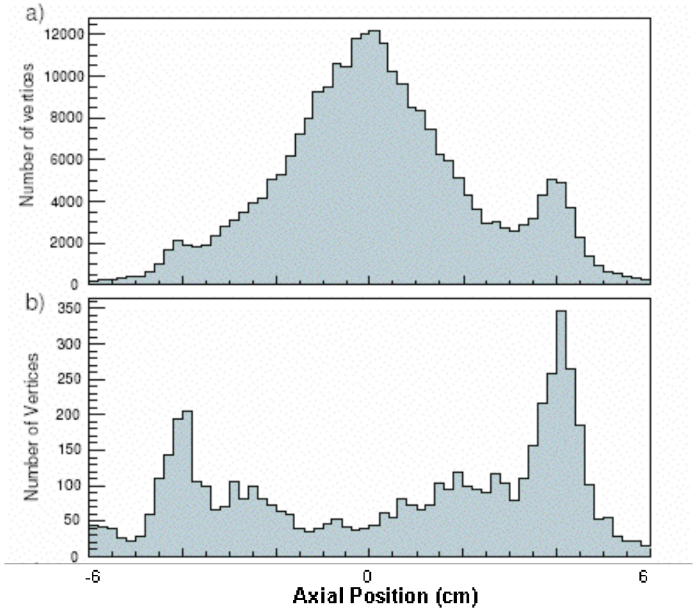

Figure 6.3: Axial (i.e. z) distribution of annihilation vertices for (a) standard cold mixing and (b) "mixing" without positrons.[31]

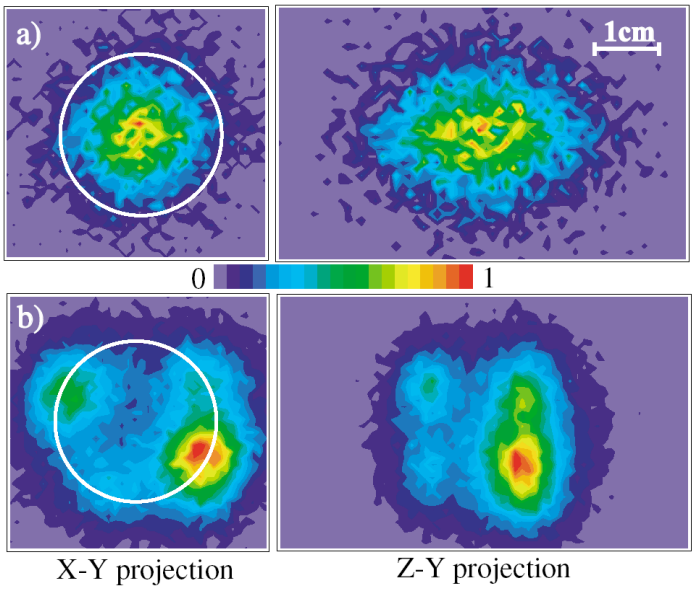

Figure 6.4: Annihilation images of trapped antiprotons in a harmonic Penning trap with (a) high residual gas density, and (b) low residual gas density. Both data are without positions. The electrode position is shown with a circle[43].

We have recently reported another effective use of the vertex imaging in trapped antiproton diagnosis[43]. Figure 6.4 shows images of antiprotons in a harmonic potential well (without positions). As shown in Fig. 6.4 (a), with a relatively high residual gas pressure of the order of 10^{-11} mbar, annihilations on residual gas dominate and images thus reflect the profile of trapped antiprotons at the time of their annihilation, an axially symmetric distribution as expected. Striking features emerge when the residual gas density is reduced to less than 10^{-13} mbar. In this case, the radial loss in the trap wall dominates over annihilation on the gas. The observed annihilation distribution is strongly anisotropic, and localized in three-dimension to a few "hot spots". Indeed, localization of antiprotons lost at the trap wall is a general feature observed in the high vacuum regime. Similar effects are seen in all trap configurations and in various different conditions used in ATHENA. The loss localization could well be universal for all charged particle Penning traps, but probably went un-noticed due to the lack of imaging capabilities until now. See Reference 43 for more details.

While these observations attracted some interest on their own from the trap physics point of view, they have profound implications for antihydrogen detection. Recall the radially symmetric distribution of annihilation at the trap wall for antihydrogen (Fig 6.2 a). The observation that *charged* particle loss at the wall results in hot spots, while the neutral antihydrogen atoms annihilate symmetrically, provides a new and effective signature of antihydrogen identification. An advantage is that we do not need to rely on the 511 keV detection, which is difficult due to its low efficiency and large background. The gamma detection was necessary for the first demonstration of antihydrogen production, but, in the recent runs of ATHENA, the presence or absence of the hot spots has been the most valuable diagnostic of our antihydrogen production processes.

6.3 Design considerations

As emphasized above, the overall design of the ALPHA experiment will be driven by the requirements for neutral atom trapping. This implies, for the Si detector, that there will be a substantial amount of superconducting magnet material between the trap and the detector. Our design goal is to retain vertex position resolution similar to ATHENA of 4 to 5 mm (σ) as illustrated in the previous section.

6.3.1 Modifications and improvements to the ATHENA detector concept

The ATHENA detector has worked well for the most part, as discussed above, and we plan to adopt its basic design features. However, several modifications and improvements are foreseen. These, along with the novel geometrical configuration of the ALPHA apparatus, necessitate construction of a completely new detector.

The ATHENA detector did not allow determination of the curvature of charged particle tracks in the 3 T magnetic field, since it only had two double-sided layers. Hence the charged tracks were approximated with straight lines, and this was a dominating factor in the vertex resolution of 4-5 mm (see below). We plan to improve the tracking in the ALPHA vertex detector by having three Si layers. The improved characterization of the charged tracks will partly compensate the resolution loss due to the multiple scattering in the extra material between the trap and the detector.

The 511 keV gamma detection will no longer be essential in antihydrogen identification for the new generation of experiments such as ALPHA, as shown in references 41 and 43. However, we will have a limited number of gamma detectors inside our magnet for the detection of trapped positrons. Transmission efficiency of 511 keV gammas through 1 cm of Cu is of order of 25%, allowing sufficient count sensitivity for diagnosis of losses from transferred and trapped positrons. We are investigating the possibility of using CdZnTe crystals for this purpose.

We envision operating the ALPHA detector at room temperature, unlike the ATHENA one, which was kept at 140K. Some of the problems encountered in the ATHENA detector, in particular, deterioration of triggering capability and a steady increase in inactive modules, may be attributed to low temperature operation and repeated thermal cycling. By operating at room temperature we hope to avoid these problems.

6.3.2 Multiple scattering

A rough estimate of multiple scattering in the ALPHA multipole magnet can be obtained from the approximate Moliere formula[10]:

$$\theta_0 = \frac{13.6MeV}{\beta cp} z\sqrt{x/X_0}\left[1 + 0.038\ln(x/X_0)\right] \qquad (6.1)$$

where θ_0 is an rms scattering angle (projected on a plane), p, βc, and z are the momentum, velocity, and charge number of incident particles, and x/X_0 is the thickness of the material in radiation lengths. In our case, z=1, β ~1, and the average pion momentum is p~300 MeV/c. Our neutral trap magnet will be made of a superconducting alloy (NbTi) and Cu. If we assume a Cu equivalent thickness of 1 cm for the scattering medium, we have θ_0~40 mrad. For a distance between the vertex and scattering material (i.e., the lever arm) of 4 cm, this corresponds to ~2 mm error in the measured track position at the vertex. This rough estimate indicates that the contribution to vertex resolution from the increased material thickness is comparable

to or smaller than the total resolution of the former ATHENA detector, the latter being dominated by the unmeasured track curvature. Therefore, if sufficiently accurate determination of the track curvature can be achieved by three or more layers of Si, the increased materials in ALPHA will be manageable in terms of vertex detection.

Detailed GEANT3 simulations have been performed to better estimate the effect of multiple scattering. Vertex resolution, defined here as the rms distance between the true vertex and the reconstructed vertex, was calculated for different thicknesses of the material between the trap and the detector. Antiprotons are annihilated on the trap wall and pions are generated with realistic phase space and branching ratios. The straight-line approximation was used for the reconstruction routine. Table 6.1 summarizes the results of this simulation study.

Table 6.1: Simulated vertex resolutions (σ) for various material thicknesses

Material Thickness Cu equivalent (mm)	Solenoid Field	Resolution x (mm)	Resolution z (mm)	Comments
1.65	3 T	4.3	1.6	ATHENA case
1.65	0 T	1.3	1.7	ATHENA- without B field
10.0	3 T	5.0	3.0	ALPHA - two Si layers
10.0	0 T	2.8	2.8	ALPHA- known track curvature

The first row is similar to the ATHENA case, where the Cu vacuum wall is 1.65 mm. That the X resolution is much worse than that in Z reflects the effect of the magnetic field. This is confirmed in the second row, where the B field is turned off, and the X resolution is substantially improved. The remaining resolution in Row 2 is due primarily to multiple scattering. This comparison of the two cases indicates that ATHENA's 4 mm vertex resolution is dominated by the unmeasured track curvatures.

The third and fourth rows are the simulations with increased scattering material. Instead of 1.65 mm, a thickness of 10 mm of Cu, which is similar to the thickness of superconducting magnet material and cryostat in ALPHA, is used in the calculations. With a 3 T solenoid field on (Row 3), the resolution is worsened compared to the standard ATHENA case (Row 1), due to increased multiple scattering, as expected. Recall that because of the straight-line fits in the track reconstruction, the track curvature is unmeasured in this case. This level of vertex resolution is expected when only two Si layers are used in ALPHA. Row 4, with no B field, isolates the effect of multiple scattering as in Row 2. The X plane resolution of 2.8 mm is in rough agreement with the estimate above using the Moliere formula. This value in Row 4 indicates that, if in a realistic ALPHA setup, the reconstruction error due to track curvature can be made negligible (e.g. by having three Si layers), a vertex resolution of the order of 3 mm can be achieved. This is well within our design goal.

The calculated distributions of the difference between true vertices and the reconstructed vertices, X(MC)-X(reconst), are graphically compared for the cases without magnetic field (Figure 6.5, left), and with the 3T solenoid field (Figure 6.5, right).

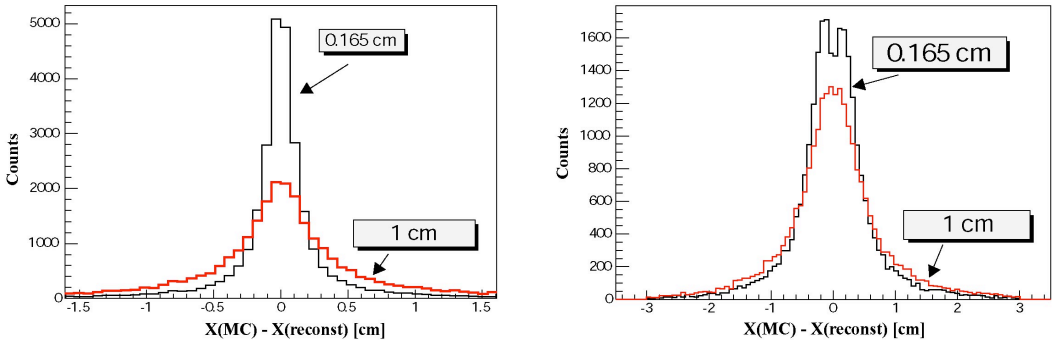

Fig 6.5: Calculated difference between the true vertices and reconstructed vertices for two different material thicknesses (as indicated in square boxes). Left: without magnetic field, Right: with 3T solenoid field.

Note that the magnitude of the multiple scattering scales only as the square root of the material thickness (see eq: 6.1), hence our conclusion here is not overly sensitive to the exact thickness of the magnet materials in the ALPHA apparatus.

6.3.3 Other effects

The effect of the multipolar field (as opposed to only the solenoidal field) on charged particle trajectories is expected to be small compared to the multiple scattering discussed above, and can in principle be accounted for, given the charge and momentum of pions, and the magnetic field distribution. A quantitative GEANT study is under way to confirm this assumption.

The increased thickness of magnet material will also result in a greater probability for the conversion of high energy gammas from neutral pion decays. The track pattern recognition routine in the off-line analysis software may need to be improved, should the increased number of charged tracks become problematic. Note that conversion events will have a rather well defined topology, since they mostly occur in the neutral trap magnet at a fixed radius.

Sufficient software expertise exists within the ALPHA collaboration to deal with these foreseeable issues.

6.4 Trigger and data acquisition

ALPHA members have been involved in the design and development of the trigger system and the data acquisition system for the ATHENA vertex detector, and we will use this as a base line. The proposed readout and trigger schemes are illustrated in Figs. 6.6 and 6.7.

A good feature of the IDEAS VA2-TA readout chip, used in ATHENA, is its self-triggering capability. In the analysis[41], it was shown that this trigger signal can be used as a proxy for the antihydrogen signal in many cases, and some important physics results were obtained using this level 0 trigger signal[35,46]. We plan to retain to this capability in ALPHA. Higher-level triggers (Figure 6.6) will apply various cuts such as multiplicity and trap conditions.

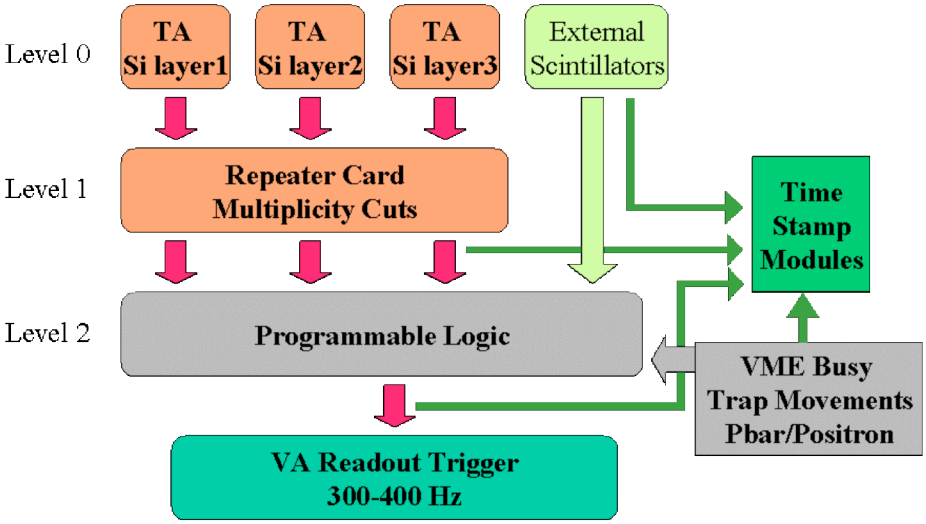

Figure 6.6: ALPHA vertex detector trigger scheme

Once the trigger is given, a VME sequencer V551 will initiate the readout of a VA chip, in which analog signals from each Si strip are stored. With a clock rate of up to 5 MHz, a sequential read out of 256 channels from one module will take of order of 100 μs or less. The analog signals are zero-suppressed, and stored in VME flash ADCs (V550), which are read out via an MXI-2 bus to a PCI bus, and recorded on a hard disc. The maximum full detector read out rate is 300-400 Hz. This is limited by the data transfer rate from the VME to the MXI bus, but if necessary, a faster rate would be possible using more modern readout systems.

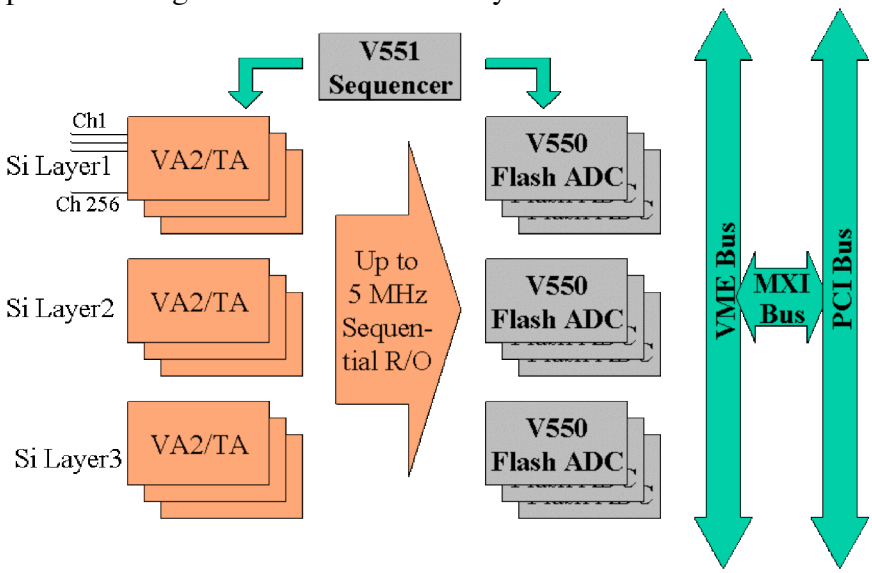

Figure 6.7: ALPHA vertex detector readout scheme

Trigger events at each level, external annihilation scintillator signals, as well as trap and other slow control activities, are time-stamped via VME multi-scalars which are synchronized to a 10 MHz atomic clock. Deadtime-free operation is possible for indefinite duration.

The ATHENA data acquisition code is currently written in National Instruments' LabView-based program, running on a Windows platform. While it is not optimal for the processing speed, particular requirements of trap experiments, where the time scale involved varies from micro seconds to hours, favours this approach.

6.5 Simulations and analysis software

For the design studies shown here, a combination of GEANT3 and GEANT4 is used at the moment. We are developing a full GEANT4 model for our physics analyses, in time for the 2006 run. On-line and off-line software will be written in C^{++} using the ROOT package, and will run on a Linux platform. The rest of the control code (traps, laser, positron source, etc.) will be written in Window's based LabView.

6.6 Detector Alignment

Relative mechanical alignment of each layer of the Si detector will be determined using cosmic rays when the magnetic field is turned off. Alignment of the detector with respect to the trap is somewhat more difficult, and we will use a method developed for the ATHENA detector[47]. Figures 6.8 and 6.9 show examples of such measurements. By moving the antiproton trap well, and measuring the annihilation positions, one can obtain the correlations between trap well positions and measured annihilation positions. The detector z-position with respect to the trap is thus determined with 1 mm accuracy, a task that is otherwise difficult to achieve in such a setup.

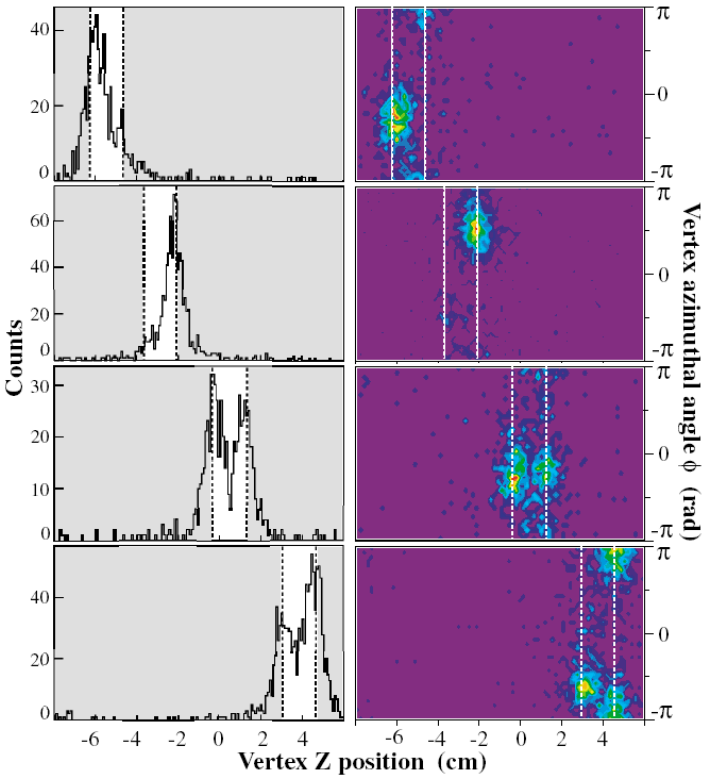

Figure 6.8: The projection of the antiproton annihilation distribution on the z axis (left column) and on the z-ϕ plane (right column) for four different confinement setups. The trap well positions are indicated by the unshaded regions, and the positions of the electrodes are depicted with dashed lines.

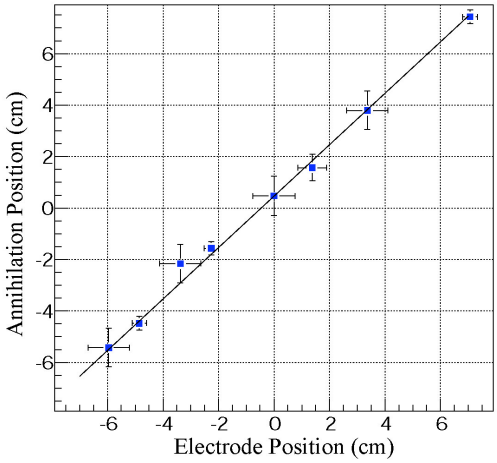

Figure 6.9: Correlation between the trap well position and the measured annihilation positions.

7.0 Positrons for ALPHA

ALPHA is fortunate in having the entire ATHENA positron apparatus available for use. It will be recalled that this instrument, based around an initial 50 mCi (1.8 GBq) ^{22}Na source moderated using a solid neon film, was capable of accumulating around 200 million positrons in a 10 minute period[14]. For the ATHENA duty cycle around 75 million positrons (300 s accumulation) were routinely available for antihydrogen formation and experimentation[12]. It should be noted that the external positron accumulator combined with transfer into the high-field, extreme high vacuum utilized in ATHENA is by far the most efficient method for accumulating large numbers of positrons in a UHV environment. The normalized accumulation rate is about 7×10^3 /s/mCi, which is about one and a half orders of magnitude higher than a recently reported accumulation method[48] and almost three orders of magnitude higher than the scheme used by ATRAP[40].

Aside from routine maintenance to the accumulator, two major upgrades will be undertaken. The ^{22}Na radioactive source in the apparatus is now over 3 years old; i.e., greater than one half-life (2.6 a) for this isotope. It is vital to have a high number of positrons available so that the antiproton cooling[46] conditions and antihydrogen formation rates are optimum. It will also be necessary to retain maximum positron accumulation capabilities into the antihydrogen trapping era, when loss of the higher temperature anti-atoms will be inevitable. The radioactive source will be upgraded to an activity of 100 mCi (3.7 GBq); such sources have recently become commercially available[49]. We expect to be able to replace the source biannually, and will write this into our funding proposal.

Furthermore, losses of 50% of the positrons on transfer from the positron accumulator to the ATHENA main magnet and nested trap arrangement were typically encountered[12]. These losses are most likely due to aperture restrictions and to subtle misalignments of the system. We expect, during the long shutdown, to be able to trace their origin and rectify this loss. Thus, we expect that 300 million positrons (200 s accumulation) will be routinely available for ALPHA when the AD restarts in 2006.

8.0 Laser Systems

The ALPHA collaboration not only has the expertise in the necessary laser systems needed for the experiment, already with a broad base of installed laser systems, but also is testing new technologies and systems for studying the antihydrogen atoms. After the trapping of the atoms, the long-term goal is to perform laser spectroscopy on the engineered 1S anti-atoms.

In 2004 the groups from Swansea, Tokyo, Aarhus and Riken, and Rio de Janeiro, all members of ALPHA, conceived and constructed a laser system to laser stimulate formation of antihydrogen in ATHENA. The data from the experiment are still being analyzed; however, no obvious enhancement was observed in the experiment in spite of favorable technical conditions. The laser was directed into the mixing region during antihydrogen formation, and it was investigated whether any enhancement of formation could be observed for different laser positions and different laser wavelengths. The wavelength with expected maximum enhancement had been found to be 10.96 μm. The current understanding is that this likely negative result is due to formation being dominated completely by the 3-body process, as also suggested by other recent work of ATHENA[31] and F. Robicheaux et al.[32] The laser had been estimated to give rise to a stimulated formation rate of ~60 Hz, under equilibrium conditions at 15 K. The spontaneous radiative combination rate was estimated to be ~ 40 Hz in ATHENA[35]. Recent work indicates that ATHENA did not have equilibrium 15 K conditions, and the expected rates should thus be significantly lower than these estimates. In light of these recent findings it is thus likely that the null-result is caused by non-ideal physical conditions and the domination of the three-body formation process.

For the trapping of antihydrogen in ALPHA, and in particular the spectroscopy to follow it is crucial to have anti-atoms in the ground state. The high angular momentum states generally formed by the three-body process are slow to decay to the ground state, and may therefore not be ideal for our future pursuits. In order to plan for this contingency ALPHA will retain the possibility of stimulating the formation, as this is a means to form antihydrogen in low quantum states. This capability will be further expanded by a build-up cavity for the CO_2 laser light, which will increase the laser intensity 10 fold. If this experiment is successful, it will be relatively easy to upgrade it to perform the first simple spectroscopy by stimulating the transition from the n=11 state reached by the CO_2 laser to the n=2 state by letting the atoms interact with a 377 nm CW laser.

The Aarhus group in ALPHA will continue its effort to construct a stabilized 243 nm laser system for two photon spectroscopy of (anti)hydrogen. The laser system is based on that used for high-resolution spectroscopy of hydrogen at MIT[50]. It consists of a Coumarin 102 dye laser pumped by a Kr^+ laser, which is then frequency doubled in a BBO crystal in an enhancement cavity to generate tens of milliwatts of laser radiation at 243 nm, the necessary wavelength for exciting the high quality factor, two-photon 1S-2S transition. The laser frequency must be actively stabilized to an external ULE cavity. The Dye-Laser (Coherent 899-21), the Kr^+ gas laser (Coherent Innova) and the doubling cavity are currently installed and working at the laser laboratory in the AD hall. The system delivers 243 nm light with a bandwidth of ~ 1 MHz. In 2005 this system will be upgraded with an external reference cavity that will help reduce the laser line width to ~1 kHz. The schematic for the final system is shown in Figure 8.1 below.

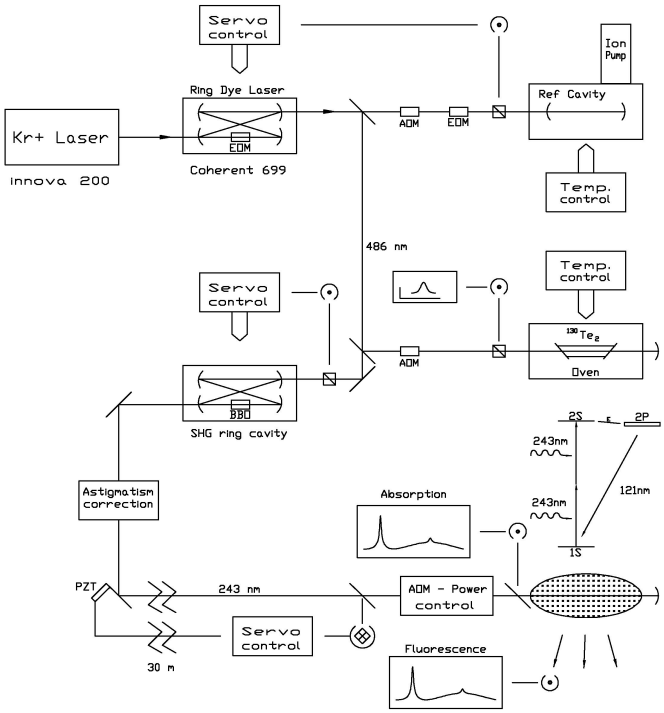

Figure 8.1: The MIT laser for 1s-2s spectroscopy of hydrogen

In parallel with this effort, a hydrogen beam experiment will be built, and will be used for benchmarking the laser system, as well as, in the future as a possible reference system for precision spectroscopy.

One desired improvement over the CW system would be, for the next phase of ALPHA, to have much higher power at 243 nm, even at the expense of a slight broadening of the laser linewidth. In particular, a microsecond Fourier transform limited pulse at much higher power of stabilized 243 nm would be quite desirable. An effort is under way in Rio to seed-inject a 10 W quasi-CW laser diode with a stabilized Ti:sapphire laser at 980 nm. If this injection seed test works well, the Rio group would be ready to invest heavily in a longer pulse, higher-power quasi-CW laser diode to be locked at 972 nm. From 972 nm the laser radiation can be frequency doubled twice, first in a $KNbO_3$ cavity, and then in a BBO cavity. Both the cavities and crystals exist already in Rio. If this system can be made to work, the Ti:sapphire/Diode laser system could be transported to Geneva, or the Aarhus dye laser system converted to Ti/sapphire.

The Calgary group has experience in pulsed hydrogen spectroscopy[51], and owns a pulsed laser system to generate approximately 15 ns pulses of 243 nm, narrow-linewidth, coherent radiation. The existing Canadian system uses a XeCl Excimer laser (308 nm) to pump a pulsed dye laser system (Coumarin 102) producing up to 250 kW of 486 nm laser radiation, which is single-pass doubled in an angle-tuned BBO crystal, producing up to 40 kW of 243 nm radiation. There are two different types of dye laser oscillators available in Calgary: a broadly scan-able transversely-pumped oscillator producing 3 GHz linewidth pulses, and a single-longitudinal mode laser oscillator that produces transform-limited nanosecond pulses but is much more difficult to scan. Dye lasers and frequency doubling components could be transferred from Calgary, but a new pump laser, preferable an internally

tripled, pulsed Nd-YAG laser, would need to be acquired. Such a laser system could be used for two-photon, resonantly-enhanced photo-ionization studies of anti-hydrogen, to clearly identify the existence of trapped 1s anti-hydrogen, and/or single photon photo-ionization studies to identify excited-state anti-hydrogen.

9.0 External Detection of Antiproton Annihilations

External detection in ALPHA will consist of three types of detectors. (1) the *Si beam detector* measures the spatial profile of antiproton beams; (2) the *external beam detectors*, made of plastic scintillators, detect the annihilation of beam antiprotons in pulsed mode and monitor the beam intensity and stability; (3) the *external annihilation detectors,* also made of scintillators, are used to study the trapped antiprotons by detecting their annihilations in single particle counting mode. The requirements for ALPHA are very similar to those of ATHENA, and we retain the expertise and experience from the latter.

9.1 Si beam detector

A thin (67 μm), segmented Si diode detector was used in ATHENA in order to measure the antiproton beam profile and to steer the antiproton beam onto the central axis of the catching trap. Due to a high current generated by a pulse of several 10^7 antiprotons, amplification of the signal was not necessary and the current across a 100 Ω resistor was directly read into a charge-sensitive ADC. In order to avoid non-linear effects such as charge recombination in Si, the detector was biased to 100 V, several times the depletion voltage. A similar beam profile detector will be used in ALPHA.

9.2 External beam detectors

The intensity of the antiproton beams entering the ALPHA apparatus will be measured via plastic scintillators, placed outside of the ALPHA main magnet. When the thickness of beam degrader is optimized for antiproton trapping, roughly half of the antiprotons in the beam will annihilate in the degrading materials. A burst of pions from such annihilations, occurring within a few hundred ns, cannot be measured in single counting mode; hence total light yields from the scintillators are read out by hybrid photodiodes (HPDs), and measured in current mode. HPDs offer a good signal linearity over a wide dynamic range, and robustness against magnetic fields. They are thus well suited for this application. A similar system was developed and successfully used for ATHENA[52]. The external beam detector will also provide the trigger signal for the fast switching of the high voltage for trapping of antiprotons.

In ATHENA, the gain of the external beam detection system was calibrated via the activation method[53,54]. Antiprotons impinging on aluminium produce $^{24}Na^*$ which then decays by gamma emission. By measuring the induced activity in Al with a calibrated Ge detector, the antiproton beam intensity can be deduced, and the beam detector signal can be calibrated in an absolute manner. A similar calibration can be performed in ALPHA. This will be complimentary to the current transformer signal in the AD transfer line, which provides information on the beam intensity immediately after the ejection septum.

9.3 External annihilation detectors

External annihilation detectors consist of plastic scintillators read out by photomultipliers. They will surround the ALPHA magnet, and unlike the beam counters, detect antiproton annihilations in *single counting mode*. The PMTs are

screened from the magnetic field by mu-metal shields and iron housings, and are mounted in a region where the stray field is small. Hardware logic circuits select the topology of annihilation events in order to enhance signal-to-background.

External annihilation detectors can be used to count the number of trapped antiprotons and to study their dynamics. For example, by slowly releasing trapped antiprotons onto a foil, and by counting the annihilations as a function of time, the energy distribution of trapped antiprotons can be deduced (see Figure 9.1), and from a series of such measurements, antiproton cooling dynamics can be studied.[46]

Shown in Figure 9.2 is an excellent correlation between the beam intensities, measured with the external beam detector, and the number of annihilations from trapped antiprotons, measured with the external annihilation detectors in ATHENA.

The external annihilation detectors must also be able to detect the annihilation of trapped antihydrogen atoms when they are released from the neutral trap. Depending on the number of anti-atoms that can be trapped and how quickly they can be released, this new detection task could set stringent new limits on the signal to noise level that is acceptable in the external detectors. This problem is currently under study, and we are investigating innovative ideas from atomic physics for releasing or dissociating trapped antihydrogen atoms in as short a time as possible.

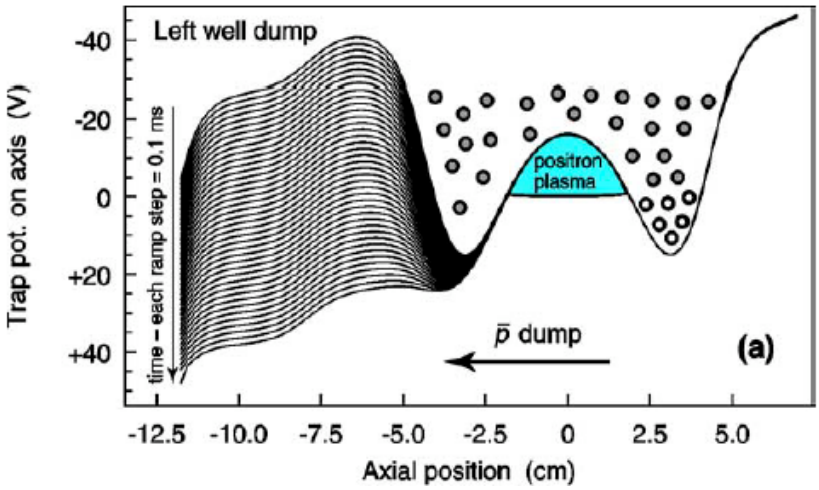

Figure 9.1: Schematic of the antiproton dump onto the degrader foil. Different on-axis potentials during the ramping are shown with lines. With the knowledge of the potentials as a function of the time, the antiproton annihilation time distribution can be converted to the energy distribution of trapped antiprotons[46].

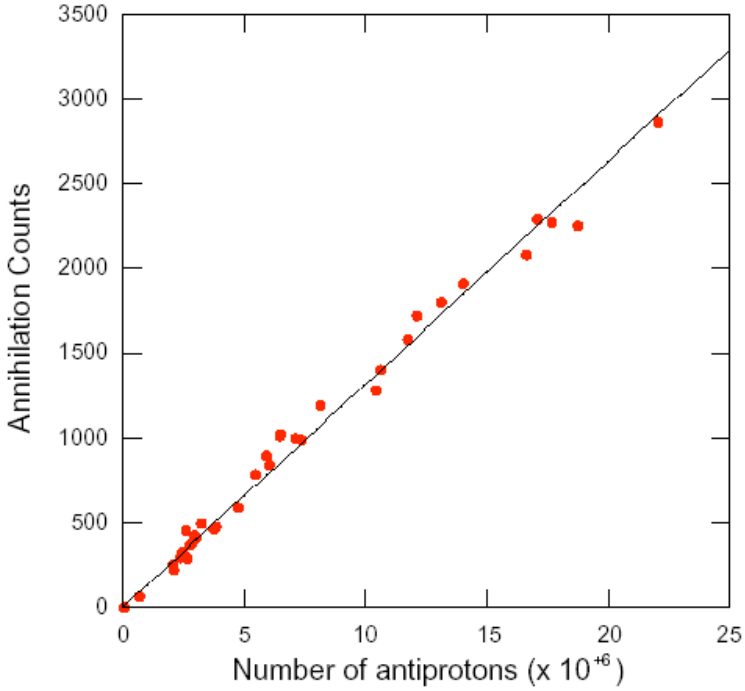

Figure 9.2: Counts measured by the external annihilation detectors upon the release of trapped antiprotons as a function of antiproton number in the incoming beam as measured by the external beam detector.

10.0 Plasma Diagnostics and Manipulations

Regardless of the mixing method used for antihydrogen production, it is crucial to know the characteristics of the constituent plasmas in detail and to be able to manipulate these. In ATHENA this was done by a nondestructive method based on measurement of the first two axial electrostatic mode frequencies[44,45]. It was thus possible to obtain information in real-time about the density, aspect ratio and temperature of the electron or positron plasma. Moreover, by comparing the exact plasma response to a resonant circuit model, it was possible to obtain the plasma length and thus also the plasma radius and total particle number. A similar system will be implemented for ALPHA. Additionally, the ability to count the total number of particles in the different plasma species using a Faraday cup will be built into the ALPHA apparatus. Furthermore, if space restrictions allow, a phosphor screen will be built into the ALPHA apparatus. This will allow study and control of plasma sizes and transverse distributions. The Faraday cup and phosphor screen will also allow useful cross-checks and calibration of the plasma modes system.

While knowledge of the detailed plasma parameters is crucial in order to understand the processes involved when producing antihydrogen, it is often also useful to be able to tailor these parameters for specific experiments. Thus in ATHENA it was possible to change the plasma size and density using a rotating electric field[27,28] applied to a split electrode in the mixing region. This “rotating wall” technique can be used to both expand and compress plasmas and thus obtain the desired plasma parameters. The use of the rotating wall causes some heating of the plasma and it is therefore necessary to have a cooling mechanism available. For electrons and positrons in a high magnetic field synchrotron cooling solves this problem. Recently the rotating wall in the ATHENA mixing trap was used to obtain a density of the positron plasma of 3×10^{10} cm^{-3}, which is the highest density for a

positron plasma ever recorded[55]. ALPHA has available all of the hardware and software used to implement the rotating wall in ATHENA.

Finally, the ability to change the temperature of the plasmas using resonant RF-heating as in ATHENA will also be implemented in ALPHA. This allows the switching off of the antihydrogen production, particularly the three-body recombination[35].

11.0 Experimental control and data logging

Experimental control in ATHENA involved the coordination of the control systems of the positron accumulator, the anti-proton catching trap and the antihydrogen formation trap with the AD cycle. Two 32-channel programmable pulse generators (Becker & Hickl PPG-100) provided the timing backbone. A master Labview program, which provided the precision timing control for the antihydrogen mixing trap potentials, controlled these. The program "requested" positrons from the positron accumulator and cold antiprotons from the catching trap. When these were received the particle mixing procedure, which lead to the formation of antihydrogen, was initiated. Voltages on the electrodes of the mixing trap were supplied by programmable triggerable DACs (100 kHz, 16-bit VME-based DACs (Joerger VDACM) with a buffer depth of 32 k steps. The sequence of required voltages was downloaded before the procedure was initiated and the pulse generator invoked the changes at the required time. Plasma manipulation instruments such as the rotating wall and plasma diagnostics such as the modes system were also triggered. An essential function of the program was to send timing flags to the data logging system so that detector events could be related to experimental manipulations. The fact that there were three systems is a reflection of the development history of the experiment rather than being a design choice.

In ALPHA the general architecture will be retained but the catching function will be integrated into the antihydrogen formation system. This will greatly simplify the system and reduce hand shaking and synchronization failures. The existing control system for the positron accumulator will be retained as the advantages of independent operation for development and optimization outweigh any synchronization issues. Furthermore an improvement in monitoring capability for the experimenter is envisaged. Although the data logging function performed accurately, an offline decoding procedure was required to review the experimental process. It is envisaged that the ALPHA control and logging program will also provide a real-time "tickertape" monitoring of all the crucial experimental parameters as an aid to the faster development of experimental experience.

12.0 ALPHA Organizational Information

12.1 Construction and Commissioning

The two new large investments, in time and money, for the ALPHA apparatus are the multipole/cryostat assembly and the silicon vertex detector. The remaining effort involves replacement or refurbishment of subsystems of the ATHENA apparatus, and, for planning purposes, ALPHA may be reasonably thought of as a major upgrade to ATHENA rather than a completely new device. Note that the ATHENA apparatus underwent extensive internal modifications after the 2002 and 2003 run periods. These were coordinated by members of ALPHA and involved complete reconstruction of the trap assembly and major modifications to the

cryosystem to allow laser access. These could be completed during a six-month shutdown of the AD. The construction of a new trap and cold assembly is thus not expected to determine the critical path, provided the BNL magnet construction proceeds without major setbacks. Indeed, we expect to have time to test the multipole assembly with electrons at Berkeley before incorporating it into the ALPHA cryostat.

As mentioned above we will finalize the multipole/mirror coil configuration by late January, 2005. The BNL experience is that winding such a magnet takes about 10 days per layer. Conservatively, and allowing for BNL engineering time, we should have a completed unit by 1 May, 2005. The cryostat will be designed and built in parallel with the magnet and should also be ready by mid-2005.

Efforts at CERN in 2005 will include upgrade of the positron trap and transfer system in the current ATHENA zone, control system and DAQ development, Monte Carlo and online software development, plasma diagnostics development, and laser system development. ALPHA has a permanent, on-site presence of at least seven physicists or students who work full time on the experiment.

The silicon detector is the longest lead-time item for the ALPHA apparatus. We will attempt to save as much time as possible by using existing sensor and chip designs, but given the complexity of the silicon detector and the lead time to develop the detector module, the detector is unlikely to be ready for installation in mid-2006. The detailed schedule for the detector construction is under development and will be communicated to the SPSC by the end of January, 2005. The apparatus is conceived to allow rapid turnaround from cold to warm states so that the detector, if completed, can be easily installed later in the 2006 run.

In lieu of the silicon detector, initial commissioning of the apparatus and production of antihydrogen can be performed with external detection and the field ionization technique[13,33].

We thus expect to have an apparatus capable of producing antihydrogen and of studying the effects of multipole and mirror fields on the trapped plasmas and on the antihydrogen production process, when the AD resumes delivery of pbars in 2006. First trapping attempts can be made in 2006, but they will be under-diagnosed until the silicon detector is delivered. We are investigating supplemental systems to aid detection in the interim.

The long-term future of the physics developments is difficult to foresee until more is known about the success of the trapping efforts. A determination of the fundamental feasibility and efficiency of trapping antihydrogen should take 2-4 years from AD start-up. The goal of precision spectroscopy and precision CPT tests is in sight but requires steady and sometimes difficult, iterative progress. This is the nature of tests of fundamental symmetries. ALPHA is committed to continuing this progress, and will be ready with the necessary laser systems when there are trapped antihydrogen atoms to illuminate.

12.2 Collaboration Capabilities

The five ALPHA institutes currently active in the AD physics program have extensive experience in all aspects of antiproton and antihydrogen physics. These institutes have long constituted a vital, active, onsite presence in the ATHENA experiment. In addition to being involved in all aspects of the ATHENA physics program, these institutes have contributed the following expertise and hardware to ATHENA:

Swansea: the ATHENA positron accumulator, positron transfer, technical coordination, plasma diagnostics and control, CO_2 laser system

Aarhus: ATHENA laser laboratory, 1s-2s laser system, technical and physics coordination, CO_2 laser system

Tokyo: external detection, trigger system, data sequencing and acquisition, CO_2 laser physics and laser system, control programming, plasma diagnostics

RIKEN: external detection, trigger system, data acquisition, CO_2 laser system

(In addition to their ATHENA activities, Tokyo and Riken are the leading institutes in the ASACUSA collaboration.)

Rio: hydrogen trapping and spectroscopy, led the MIT experiment for cold hydrogen trapping and spectroscopy, laser development for precision spectroscopy

The above institutes have, in the past year, accounted for about 70% of the on-site presence in ATHENA. They have handled all of the coordination of the experimental and technical activity since 2001.

The five new institutes in ALPHA have capabilities to supplement those listed above.

The Liverpool group has extensive experience in design and fabrication of Si microstrip detectors, and will lead this effort in ALPHA. Its nationally funded facility, Liverpool Semiconductor Detector Centre, is involved in construction of other state-of-the-art Si detectors such as the ATLAS semiconductor tracker (SCT) and the LHCb vertex detector (VELO). The group also has longstanding expertise in sophisitcated gamma detectors (including scintillators and CdZnTe), data acquisitions sytems, detector and system modelling using GEANT and in all aspects of experimental nuclear physics.

The Berkeley group has a strong, internationally respected tradition in non-neutral plasma physics, both experimental and theoretical. They have a complete laboratory for parallel studies of trapped, cryogenic plasmas. This laboratory was used to conduct the quadrupole measurements described here, and will be used for fast turnaround studies in support of ALPHA. They have been active in research related to antihydrogen production for several years, and have identified some of the key issues for the future of the field[20,21,22].

TRIUMF, as a national infrastructure lab for the Canadian High Energy Physics community, has expertise in various types of detectors as well as the related software and simulations. The group is lead by a former ATHENA physicist who, until recently, has been onsite and active in the CERN AD physics program since its inception (see Tokyo and Riken above). New members have experience in precision Penning trap experiments, DAQ, tracking software and GEANT simulations.

The Calgary group adds a new capability in pulsed laser physics to ALPHA. Their collection of lasers and cavities for pulsed hydrogen spectroscopy should play an important intermediate role between the first trapping and the long-term goal of

spectroscopy with the highest possible precision. The prospects for laser-based diagnostics of trapping and of the antihydrogen state are intriguing new perspectives to be pursued by this group.

The Manitoba group has extensive experience in atomic physics at storage rings, including precision laser spectroscopy, atomic recombination, and laser stimulated recombination. They also have expertise in laser cooling and trapping of small numbers of radioactive atoms.

With the above capabilities and the institutes' record of securing funding, we are confident of developing and constructing a competitive apparatus for the next phase of AD physics. In actual numbers of man-years of active participants, the size of ALPHA should be comparable to that of ATHENA.

12.3 Budget and Financing

12.3.1 Budget

The following budget outline comprises three sections, the running, replacement and new investment costs. These are reported as cost per year. Assuming the participation of 20 physicists at post doc level or above the cost per physicist is also given. The budget does not include; salaries for physicists, support for students, workshop costs at participating institutes, travel or relocation allowances. In the case of large investment items the cost is divided over five years. Cash flow concerns due to the fact that the investment in large items will be made at the beginning of the period will need to be addressed by careful planning. The period covered is from 1st January 2005 to 31st December 2009.

Running costs (Common fund)

Operator	65 kCHF
Electronics pool	35 kCHF
Cryogens	10 kCHF
Maintenance	7 kCHF
Computers	4 kCHF
Printing	1 kCHF
Fax & Telephones	2 kCHF
Consumables	2 kCHF
Total	126 kCHF/year
	6.3 kCHF/physicist/year

These estimates are based on experience during ATHENA. Since there will be no machine operation in 2005, the question arises as to whether payment for the operator is due in that year. Over the five-year planning period the electronics pool is projected to consume 175,000 CHF. Despite some of the attractions of using the pool, (defective instrument replacement, no obsolescence problems) the scope and nature of the required electronics items is now well known. Consideration should be given to purchasing some items outright rather than hiring from the electronics pool.

Replacement investment

ALPHA retains much of the core equipment from ATHENA including the complete positron accumulator, complete laser systems for stimulated recombination and 1s-2s spectroscopy as well as the superconducting solenoid with its ancillary

vacuum equipment. A second superconducting solenoid, with similar field quality and strength but with a larger bore, is owned by a member of the collaboration. The detector is listed under new investment as it is a new design.

What follows is not detailed and because of this it is conservatively costed.

Cryogen handling	25 kCHF
Scintillators+PMT's	50 kCHF
Trap potential control	15 kCHF
Computer cards	12 kCHF
Trap high voltage	10 kCHF
Data logging equipment	5 kCHF
Mode diagnostics	10 kCHF
Electron gun	5 kCHF
HPD's + scintillators	15 kCHF
Total	147 kCHF

New investment

Detector

Silicon	150 kCHF
ADC	100 kCHF
Mechanical support	50 kCHF
Repeater card	20 kCHF
Power supplies	10 kCHF
Technician (2 years)	120 kCHF
Total	450 kCHF

The silicon and ADC costs are based on experience with the ATHENA system. We are investigating new less expensive possibilities for the ADC's. Technician costs are included due to the very specialized nature of this work.

Multipole magnet

Winding	140 kCHF
Power supply	100 kCHF
Cryostat	100 kCHF
Helium system	20 kCHF
New traps & cabling	20 kCHF
Total	380 kCHF

The costs for the winding and cryostat are based on the experience of BNL in previous projects for DESY and BEPCII. It is envisaged to avail of CERN expertise in the design of the cryostat. The trap and cabling cost is included here because the magnet has made this change necessary.

Total investment cost	977 kCHF	
Total running cost	630 kCHF	
Grand total	1.6 MCHF	320 kCHF/year
		16 kCHF/physicist/year

12.3.2 Financing

Given the current situation and the historical success rate of the ALPHA institutes in obtaining funding, the running costs and most of the investments can be covered without major new grants. The exception is the silicon detector, which will be included in a new, joint, grant proposal by Swansea and Liverpool. The application for this grant is being prepared now and will be submitted in early 2005. The investment for the multipole can be covered under existing grants, and its impact is ameliorated somewhat by the lack of running of the AD in 2005 and the first half of 2006.

Acknowledgements

We would like to thank Professor Alberto Rotondi for performing the Monte Carlo calculations in Section 6, Dr. Stefan Russenschuck and Bernhard Auchmann for help with ROXIE, and Dr. Michael Harrison and the rest of the BNL Superconducting Magnet Group for many useful discussions.

References

[1] ALPHA Letter of Intent, SPSC-2004-026
[2] J. Fajans, W. Bertsche, K. Burke, S.F. Chapman, and D.P. van der Werf, submitted to Phys. Rev Lett.
[3] G. Luders, Ann. Phys. **2** (1957) 1.
[4] See for example, Proc. of 2nd Meeting on CPT and Lorentz Symmetry, ed. V.A. Kostelecky (World Scientific, Singapore , 2002).
[5] J. Ellis, J. Lopez, N.E. Mavromatos, D.V. Nanopoulos, Phys. Rev. D **53** (1996) 3846.
[6] N. Arkani-Hamed, S. Dimopoulos, G. Dvali, Phys. Lett. B **429** (1998) 246.
[7] A.D. Dolgov, Ya.B. Zeldovich, Rev. Mod. Phys. **53** (1981) 1.
[8] O. Bertolami *et al*., Phys. Lett. B **395** (1997) 178.
[9] H. Murayama and T. Yanagida, Phys. Lett. B **520** (2001) 263.
[10] Particle Data Group, Review of Particle Physics, Phys. Lett. B **592**, 1 (2004).
[11] M. Kobayashi and A. I. Sanda, Phys. Rev. Lett. **69** (1992) 3139.
[12] M. Amoretti *et al*., Nature **419** (2002) 456.
[13] G. Gabrielse *et al*., Phys. Rev. Lett. **89** (2002) 213401
[14] M. Amoretti *et al*., NIM A **518** (2004) 679
[15] D.E. Pritchard, Phys. Rev. Lett. **51**, 1336 (1983); see also Reference 1, the ALPHA LOI.
[16] B. Deutch, F. Jacobsen, L. Andersen, P. Hvelplund, H. Knudsen, M. Holzscheiter, M. Charlton, and G. Laricchia, Physica Scripta. **T22**, 248 (1988).
[17] G. Gabrielse, L. Haarsma, S. Rolston, and W. Kells, Phys. Lett. A **129**, 38 (1988).
[18] G. Gabrielse, A. Speck, C. Storry, D. L. Sage, N. Guise, D. Grzonka, W. Oelert, G. Schepers, T. Sefzick, H. Pittner, *et al*., Phys. Rev. Lett. **93**, 073401 (2004).
[19] T. M. O'Neil, Phys. Fluids **23** 2216 (1980.)
[20] E. Gilson and J. Fajans, in *Non-neutral plasma physics III*, edited by J. Bollinger, R. Spencer, and R. Davidson (AIP, 1999), **498**, p. 250.
[21] E. Gilson and J. Fajans, Phys. Rev. Lett. **90**, 015001 (2003).
[22] J. Fajans and A. Schmidt, NIMA **521**, 318 (2004).
[23] M. Holzscheiter, M. Charlton, and M. Nieto, Physics Reports **402**, 1 (2004).
[24] T. Squires, P. Yesley, and G. Gabrielse, Phys. Rev. Lett. **86**, 5266 (2001).
[25] G. Gabrielse, Adv. At. Mol. Opt. Phys. **50** (2004), to be published.
[26] C.H. Storry *et al*., Phys. Rev. Lett. **93**, 263401 (2004).
[27] X.-P. Huang, F. Anderegg, E. Hollmann, C. Driscoll, and T. O'Neil, Phys. Rev. Lett. **78**, 875 (1997).
[28] R. G. Greaves and C. M. Surko, Phys. Rev. Lett. **85**, 1883 (2000).
[29] See the BNL website: http://www.bnl.gov/magnets/BEPCII/BEPCII.asp
[30] ROXIE, © CERN 2000, S. Russenschuck et al.
[31] N. Madsen *et al*. "Spatial Distribution of Cold Antihydrogen Formation", accepted for publication in Phys. Rev. Lett. (2005).
[32] F. Robicheaux, Phys. Rev A **70** (2004) 022510
[33] G. Gabrielse *et al*., Phys. Rev. Lett. **89** (2002) 233401
[34] C. Regenfus NIM A **501** (2003) 65
[35] M. Amoretti *et al*., Phys. Lett. B **583** (2004) 59
[36] J.W. Humberston *et al*., J. Phys. B: At. Mol. Phys. **20** (1987) L25
[37] M. Charlton, Phys. Lett. A **143** (1990) 143
[38] B.I Deutch *et al*., Hyperfine Interactions **76** (1993) 153
[39] E.A. Hessels *et al*., Phys. Rev. A **57** (1998) 1668
[40] J. Estrada *et al*., Phys. Rev. Lett. **84** (2000) 859
[41] M. Amoretti *et al*., Phys. Lett. B **578** (2004) 23
[42] F. Robicheaux, Private Communications (2004)
[43] M. C. Fujiwara *et al*., Phys. Rev. Lett. **92**, 065005 (2004)
[44] M. Amoretti *et al*., Phys. Rev. Lett. **91**, 055001 (2003).
[45] M. Amoretti *et al*., Phys. Plasma **10**, 3056 (2003).
[46] M. Amoretti *et al*., Phys. Lett. B **590**, 133 (2004).
[47] M. C. Fujiwara *et al*., *Non-neutral Plasma Physics*, eds. M. Schauer et al., (AIP, New York, 2003) Vol. 5, p. 131.
[48] N. Oshima, *et al*., Phys. Rev. Lett. 93, 195001 (2004).
[49] R. Krause-Rehberg *et al*., NIM B **221**, 165 (2004).

[50] C. L. Cesar, MIT Phd Thesis, unpublished (1995).
[51] R.I. Thompson, B.P. Stoicheff, G.Z. Zhang, K. Hakuta, Appl. Phys. B **60**, S129-S139 (1994).
[52] M. C. Fujiwara and M. Marchessotti, Nucl. Instrum. Methods A **484**, 162-173 (2002).
[53] Asacusa Collaboration, private communications (2000).
[54] M. C. Fujiwara, ATHENA Technical Report (2000).
[55] L. V. Jørgensen, *et al.*, submitted to Phys. Rev. Lett.

A Trapping of Antihydrogen in ALPHA

A.1 Introduction

After a short introduction to the method and the math, a series of calculations of the fraction of antihydrogen that can be trapped as a function of well depth (in Kelvin) and antihydrogen temperature is calculated.

A.2 Distributions

The distribution of antihydrogen velocities without rotation are assumed to be given by a Maxwellian

$$f_v(v_x, v_y, v_z) = \frac{1}{(2\pi)^{3/2}\sigma_x\sigma_y\sigma_z} \exp\left[-\frac{1}{2}\left(\frac{v_x^2}{\sigma_x^2} + \frac{v_y^2}{\sigma_y^2} + \frac{v_z^2}{\sigma_z^2}\right)\right] \tag{A.1}$$

where $\sigma_{x,y,z}$ are the thermal velocities given by

$$\sigma_{x,y,z} = \sqrt{\frac{k_B T_{x,y,z}}{m_p}} \tag{A.2}$$

where k_B is Boltzmans constant, m_p is the (anti)proton mass and $T_{x,y,z}$ the temperatures in each degree of freedom. We sometimes use the terms $T_\perp$ and $T_{||}$ as the transverse (perpendicular) and axial (parallel) temperature. The system is presumed cylindrical with a strong coupling of the transverse degrees of freedom (from our solenoid magnet). The two components are given by

$$T_\perp = \frac{1}{2}\left(T_x + T_y\right) = \frac{m_p}{k_B}\sigma_\perp^2 = \frac{m_p}{2k_B}\left(\sigma_x^2 + \sigma_y^2\right) \quad T_{||} = T_z \tag{A.3}$$

where $\sigma_x = \sigma_y = \sigma_\perp$ when this terminology is used.

To simulate the influence of cross field drift in a radial electric field and an axial magnetic field we can impose a cross field azimuthal velocity to the particles. This velocity is position dependent, and we therefore need an assumption about the size and shape of the antihydrogen formation region. For this purpose we use the program used for the calculations in Ref. [1]. In this calculation we make a sample of antihydrogen atoms (typically 10^6) and give them a spatial distribution and velocities from a Maxwellian distribution, using the spatial distribution we can then add a rotational component to each atom as a function of its position. The resulting 3D velocity distribution can then be used to calculate the number of antihydrogen trapped by simple counting.

A.3 Trapped Antihydrogen

The fraction of trapped antihydrogen η of temperature T is a trap of depth T_d is in the non rotating, Maxwellian case, under the assumption that there is no

dependence on initial position[1] and full mixing of the three degrees of freedom, given by

$$\eta = 8 \int_0^{\sigma_D} \int_0^{\sqrt{\sigma_D^2 - v_z^2}} \int_0^{\sqrt{\sigma_D^2 - v_z^2 - v_y^2}} f_v(v_x, v_y, v_z) dv_x dv_y dv_z \tag{A.4}$$

where $\sigma_D = \sqrt{3 T_D k_B / m_p}$ is the trap escape velocity.

Under most circumstances we would expect (though not hope) that $T_d \ll T$ and we can approximate the above calculation with the expression

$$\eta_{T_d \ll T} = \sqrt{\frac{6}{\pi}} \left(\frac{T_d}{T} \right)^{3/2} \sim 1.38 \times \left(\frac{T_d}{T} \right)^{3/2} \tag{A.5}$$

If the longitudinal temperature ($T_{||}$) is different from the transverse ($T_\perp$) the approximate expression above changes to

$$\eta_{T_d \ll T_\perp, T_{||}} \sim 1.38 \times \left(\frac{T_d^{3/2}}{T_\perp \sqrt{T_{||}}} \right) \tag{A.6}$$

Figure 1 shows how the trapped fraction varies with the depth of the trap for a given temperature and also how it varies with temperature for a given trap depth for a Maxwellian velocity distribution.

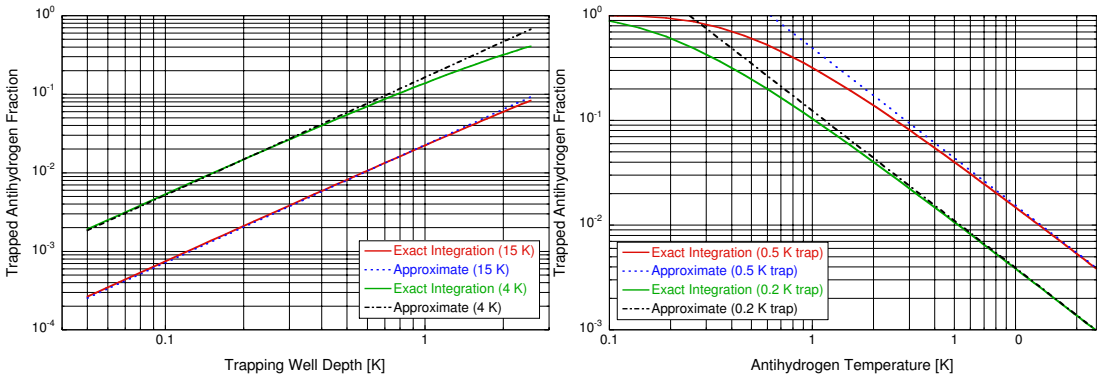

Figure 1: Fraction of antihydrogen trapped with isotropic Maxwellian temperature distributions.

If the antiprotons exhibit cross field drift we need position information and it is no longer possible to work analytically as mentioned before. The radial electrical field from the trapping potential is of order 150 V/m (at a radial distance of 2.5 mm), whereas the field from the positron plasma can be estimated by (assuming that $r_{e^+} \ll l_{e^+}, r_{elec}$ where, r_{e^+} is the plasma radius, l_{e^+} the plasma length and r_{elec} the electrode radius).

$$E_{e^+}(r) = \frac{n_{e^+} e}{2\epsilon_0} r \tag{A.7}$$

[1]This is not necessarily a good assumption, this issue will be addressed later

which for a typical plasma densities of $n_{e^+} = 1.7{\times}10^8$ cm^{-3} and radius of $r_{e^+} =$ 2.5 mm gives a field at the radial edge of 3.8 kV/m.

The $\mathbf{E} \times \mathbf{B}$ drift velocity is given by

$$v_{E\times B}(r) = \frac{E(r)}{B} \tag{A.8}$$

when the fields are perpendicular. For the example above this means a velocity of 1.3 km/s at the edge of the positron plasma (see also Ref. [1]).

The rotation due to the trap potentials alone (ignoring the fields from the particles) corresponds to a temperature of $\sim$ 0.3 K, negligible compared to expected antihydrogen temperatures. However, the space charge induced rotation is not negligible, and we have included it in the calculations in Figure 2. In this calculation the antihydrogen atoms were distributed homogeneously throughout the volume of the positron plasma, and assigned rotational components corresponding to their radial position.

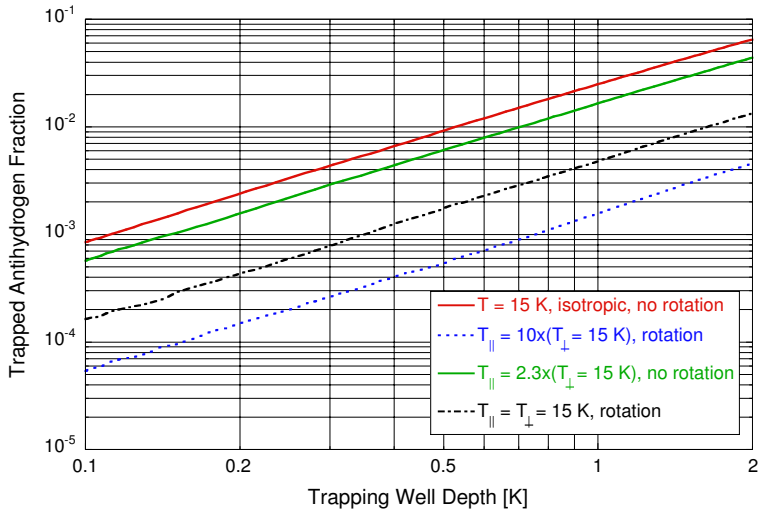

Figure 2: Fraction of antihydrogen trapped under a variety of circumstances. Note that at 15 K $\mathbf{E} \times \mathbf{B}$ rotation due to the e^+ plasma space charge reduces the trapping efficiency by a factor $\sim$6. The dotted line corresponds to the situation in ATHENA [1].

A.4 The ALPHA setup

Possible ALPHA experimental parameters are a magnetic field of 1-2 Tesla, a cryogenic environment of 4 K, a magnetic trap of 0.5 K, and positron plasma parameters comparable to ATHENA, although there are several reasons to have a reduced positron plasma density. The expected trapping fractions under these circumstances are summarized in Table 1.

We note that due to the inverse square dependence on the B-field, the trapped fraction scales as B^2 when the rotation velocity is large compared to the thermal velocity. This may be important to keep in mind when choosing the B-field.

B = 1 T, T = 4 K, T_d = 0.5 K, $n_{e^+} = 1.7\times10^8$, r_{e^+} = 2.5 mm		
Rotation Velocity	$v_{E\times B}(r_{e^+})$	3.9 km/s
Fraction Trapped	η	0.044 %
B = 2 T, T = 4 K, T_d = 0.5 K, $n_{e^+} = 1.7\times10^8$, r_{e^+} = 2.5 mm		
Rotation Velocity	$v_{E\times B}(r_{e^+})$	1.9 km/s
Fraction Trapped	η	0.16 %
B = 3 T, T = 4 K, T_d = 0.5 K, $n_{e^+} = 1.7\times10^8$, r_{e^+} = 2.5 mm		
Rotation Velocity	$v_{E\times B}(r_{e^+})$	1.3 km/s
Fraction Trapped	η	0.37 %

Table 1: Possible ALPHA senarios and the corresponding expected trapping fraction.

This scaling also implies that the trapped fraction scales as $n_{e^+}^{-2}$. Low positron densities are therefore desirable for trapping.

A.5 Magnetic Trap Configuration

In the previous calculations we neglected the initial position of the antihydrogen, except when we included cross field rotation. The assumption is not necessarily a good one. The antihydrogen potential in our magnetic trap has the following radial dependence (ignoring axial variations (mirror coils and finite length)).

$$U_{\bar{H}}(r) = \mu\left\{\sqrt{\left[B_W\left(\frac{r}{r_0}\right)^{s-1}\right] + B_z^2} - B_z\right\} \tag{A.9}$$

where B_W is the magnetic field at the wall, which for the range of magnet choices we have discussed can be taken as a constant independent of our configuration. B_z is the solenoidal field. r_0 is the trap radius. s is the multipole order, $s = 2$ is a quadrupole. μ is the magnetic moment, equal to the Bohr magneton μ_B for antihydrogen in the ground state.

Figure 3 shows the necessary wall field as a function of the solenoid field for a desired trap depth of T_D = 0.5 K. This field is given by

$$B_W(T_D) = \sqrt{\left(\frac{k_B T_D}{\mu_B} + B_z\right)^2 - B_z^2} \tag{A.10}$$

Intuitively we see that antihydrogen formed with a radial distance r from the center, will be formed with a non-zero potential energy, i.e. they must initially be colder to be trapped. The influence of this is of course largest for the quadrupole, another reason not to chose a quadrupole magnet. This is only worsened by the fact that the rotation increases with radius, and thus the effective temperature. Assigning a trap depth that depends on radius we can include this effect in the previous numerical calculations. The trap depth for antihydrogen formed at a

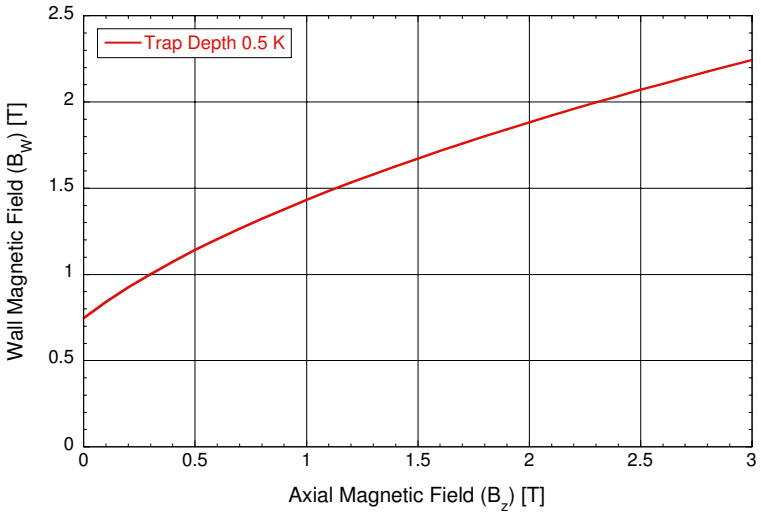

Figure 3: Necessary wall magnetic field (B_W) to form a magnetic trap of 0.5 K depth as a function of the solenoidal field. Mirror coils were not included.

radial position r is given by

$$T_D(r) = \frac{\mu_B}{k_B}\left\{\sqrt{B_W^2 + B_z^2} - \sqrt{\left[B_W\left(\frac{r}{r_0}\right)^{s-1}\right]^2 + B_z^2}\right\} \tag{A.11}$$

where $\mu_B/k_B = 0.67$ K/T. Figure 4 shows the trap depth of antihydrogen formed at a specific radius for a wall field corresponding to a maximum trap depth of 0.5 K.

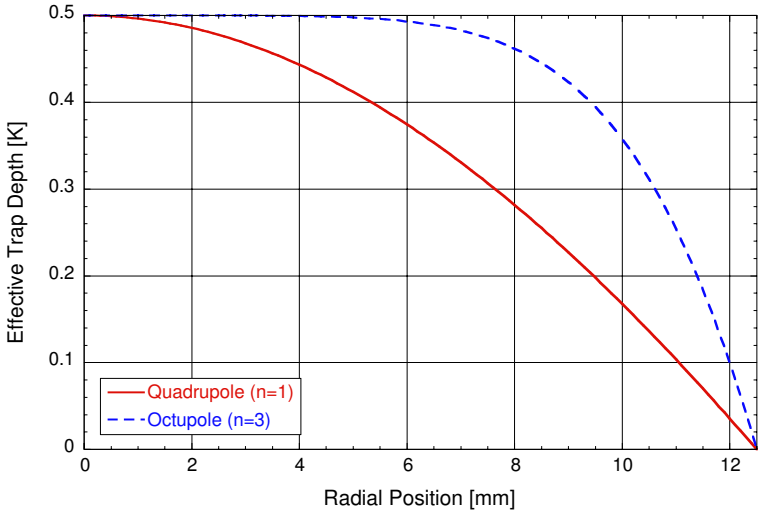

Figure 4: Effective trap depth for antihydrogen formed at different radii in a magnetic multipole trap. $B_z = 3$ Tesla. $r_{elec} = 12.5$ mm.

With a homogeneous formation region of radius r and no rotation the average well depth can be calculated by integrating the equation above. For $r = 2.5$ mm

with $r_{elec} = 12.5$ mm, the reduction in well depth is of order 2-3% for a quadrupole, and about 0.07% for a sextupole. The relative change in the trapped fraction is similar. The effect obviously increases with increasing size of the formation region, but does not seem critical in our parameter range.

A.6 Summary

We find that using the positron density in ATHENA is not desirable as it leads to very low trapping efficiencies (less than .4% for typical ALPHA parameters) due to the $\mathbf{E} \times \mathbf{B}$ drift this will induce on the antiprotons. Figure 5 shows the trapping fraction as a function of positron density. Note, that for higher densities the decreased trapping fraction stems from the fact that antihydrogen formed at larger radii is no longer trapped due to the $\mathbf{E} \times \mathbf{B}$ drift . In the regime where the $\mathbf{E} \times \mathbf{B}$ drift is important we find that the trapped fraction scales as B^2. Thus, if we wish to start out at ATHENA e^+ parameters we should use the highest possible B-field. With lower densities, when rotation becomes negligible, it should be feasible to trap ~ 5 %. We have not discussed the different well depths that will be experienced by atoms in different quantum states.

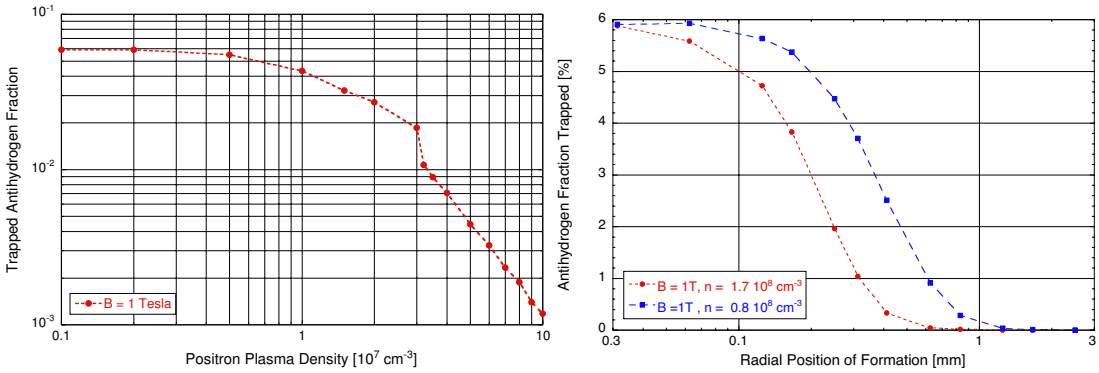

Figure 5: Trapped fraction of antihydrogen atoms. Trap depth 0.5 K. Formation at 4 K, homogeneously in a positron plasma of radius 2.5 mm, length 32 mm. Field and density as given. Left plot shows average for antihydrogen formed homogeneously over the positron plasma radius. Right plot shows the fraction trapped as a function of the radial position of formation.

References

[1] N. Madsen *et al*, Accepted for Phys. Rev. Letts. (2005)